Available online at www.sciencedirect.com
ScienceDirect
International Journal of Pharmaceutics 351 (2008) 74–91
INTERNATIONAL JOURNAL OF PHARMACEUTICS
www.elsevier.com/locate/ijpharm

Solubility of molecular crystals: Polymorphism in the light of solubility theory

P. Bennema [b], J. van Eupen [b], B.M.A. van der Wolf [a], J.H. Los [a], H. Meekes [a,*]

[a] *IMM department of Solid State Chemistry, Radboud University Nijmegen, Toernooiveld 1, 6525 ED Nijmegen, The Netherlands*
[b] *Synthon BV, Nijmegen, The Netherlands*

Received 13 June 2007; received in revised form 21 August 2007; accepted 17 September 2007
Available online 25 September 2007

Abstract

The thermodynamic theory of solubility of molecular crystals in solvents is reviewed with an emphasis on solutes showing polymorphism as in case of many pharmaceuticals. The relation between solubility and binary phase diagrams of the solute solvent system is treated. The astonishing variety of possible solubility curves as a function of temperature is explained using simple models for the solution thermodynamics assuming no mixing between the solvent and solute in the solid phase, though including the case of solvates or pseudo polymorphs. In passing a new method is introduced that allows to estimate the transition temperature of enantiotropically related polymorphs from melting temperatures and enthalpies of the polymorphs.

Keywords: Solubility; Pharmaceuticals; Regular solution; Polymorphism; Phase diagrams

1. Introduction

The first practical understanding of solubility dates back to 1900–1930 (Hildebrand, 1916, 1929; Mortimer, 1922). Since the introduction of the concept of a regular solution by Hildebrand (1929), later resulting in the solubility parameter and Scatchard–Hildebrand theory of regular solutions, numerous new models have been proposed in order to describe the non-ideal behavior of solutions more correctly. Predictive methods can be very useful tools to reduce the amount of experiments needed to determine solubilities, and the development of reliable, transferable and quick methods is in continuous progress (Gmehling, 2003a, b). Although it might seem as if 1930 is long ago, the theories described before that date still contain the essentials of current solubility models. Modern models have astonishing capabilities, but they are not complete and experimental data are still needed. Especially for multicomponent mixtures, however, experimental methods are not only time-consuming (Gmehling, 2003a), but expensive and difficult as well.

Compared to vapor liquid equilibria (VLE), much less attention has been given to SLE (solid liquid equilibria) and solubility, one of the reasons being the much larger importance of rectification as compared to crystallization (Gmehling, 2003b; Jakob et al., 1995). Still, SLE and solubility of solids in liquids are of great interest: crystallization processes are used, e.g. for the separation and purification of thermo labile compounds or isomeric compounds with a very similar vapor pressure (Lohmann et al., 1998). Moreover, the link between solid phase diagrams and solubility is rarely recognized in literature and certainly not generally known. Of course, for solubility behavior showing complete eutectic behavior, it is not so relevant to make this link, but when polymorphism occurs, phase diagrams are becoming useful. Especially for pharmaceutical compounds both fields, solubility of organic compounds in various solvents and polymorphism, have attained an increasing interest in recent years as both are essential, for instance during the development of a new drug (Ruelle et al., 2000).

It is the aim of this paper to make the connection between (binary) phase diagrams and solubility starting from simple thermodynamics relevant for the solubility behavior of solids in liquids and to apply it to the solubility of polymorphic forms. In that light it is not the aim to describe predictive models for the solubility of molecular crystals but rather to use simple models to

* Corresponding author.
E-mail address: Hugo.Meekes@science.ru.nl (H. Meekes).

0378-5173/$ – see front matter © 2007 Elsevier B.V. All rights reserved.
doi:10.1016/j.ijpharm.2007.09.021

describe the thermodynamics behind the astonishing variety of solubility curves found in practical situations. The relation with polymorphism of molecular crystals will be emphasized. Starting from the simplest of all models, the ideal solution model, the complexity of the models will be gradually increased, in all cases limiting the analysis to the essentials.

The need for quantitative solubility data, on the other hand, has led to a variety of models for predicting solubility, each with its specific emphasis; in the following a short overview is given. The first widely applicable predictive model for solubility and solutions is the regular solution theory (Gmehling, 2003a). This method makes use of a single solubility parameter, which can describe the real behavior of mixtures of non-polar compounds (Prausnitz et al., 1999). A disadvantage is that the regular solution assumptions cannot describe mixtures of polar molecules, and although some empirical modifications can extend the use of the regular solution model (Barton, 1975)(a well known example is the Hansen solubility parameter approach (Hansen, 1969)), it is in many cases replaced by more sophisticated methods. Nowadays, the modified UNIFAC(Do) method (Lohmann et al., 2001) is in general the most used method available for predictions. In 1978 already it has been shown that the original UNIFAC is capable of predicting SLE and solubility (Gmehling et al., 1978), but only for a limited number of compounds. Originally, UNIFAC, being based on a large database of thermodynamic data, was developed for VLE in the temperature range 290–400 K and predictions for SLE or below 290 K can lead to poor results. To increase the temperature range, in modified UNIFAC(Do) the temperature dependence was incorporated and SLE data were used as supporting information, improving the results considerably (Lohmann et al., 2001). For simple compounds, modified UNIFAC(Do) is a helpful tool for predicting solubility (Eckert and Klamt, 2002), but for more complicated molecules, other models have to be used. An example from the pharmaceutical field is the mobile-order-disorder theory, a relatively unknown method that can describe solubility behavior of complex drug-based molecules (Ruelle et al., 2000). Another upcoming approach is predicting real solution behavior with the help of quantum-chemical methods, such as COSMO-RS (Eckert and Klamt, 2002). Such models can describe more systems than database-limited methods such as UNIFAC, but they are not yet sophisticated enough for accurate applications (Eckert and Klamt, 2002; Arlt et al., 2004).

Despite the advances that have been made, the predictive capability for solubility is still limited. UNIFAC and modified UNIFAC(Do), for example, both make use of equations derived for eutectic systems and although most SLE are indeed eutectic (Fiege et al., 1996), systems with for example peritectic behavior cannot be described. The main reason for this limitation is that these models have been developed for temperature ranges relevant for VLE phase diagrams; extension to solid, solid–liquid or solid–solid behavior is difficult. Little attention has been given to SLE or solubility compared to VLE, but still much less attention has been given to the mixing properties in solids.

In the following sections first the link between the thermodynamics of solubility and SLE phase diagrams will be treated. Using the thermodynamic basis underlying these phase diagrams a number of models, which highlight various solubility curves one can encounter, will be analyzed. Finally, the models will be generalized, to include the cases of polymorphism and solvates.

In all cases equilibrium phase diagrams are treated, that is, kinetic effects have been neglected. Especially for crystallization using fast cooling, kinetics cannot be neglected. In recent work, Los et al. have developed methods to determine kinetic phase diagrams. For that the reader is referred to Los et al. (2002, 2007) and Los and Matovic (2005).

For solutes that have a chiral center, which is of indisputable relevance for pharmaceuticals, the reader is referred to the book by Jacques et al. (1994).

2. The theory of solubility

In this section the thermodynamic background of solubility theory is treated. A rigorous thermodynamic derivation of the solubility of a solid phase in a solvent up to the case of (quasi) regular solutions is given. For the latter a mean field model is used. Special emphasis is put on the relation between solubility curves and phase diagrams.

2.1. Solubility and phase diagrams

To discuss the relation between solubility curves and S(olid)–L(iquid) phase equilibria first a typical S–L phase diagram is discussed briefly. For a treatment of the thermodynamics of phase diagrams in general the reader is referred to the excellent book by Stølen and Grande (2004). The discussion is limited to the case of binary mixtures of compounds A and B, without loss of generality. When these compounds, besides in the liquid phases, also mix in the solid phases, a situation which is in contrast with the case of solubility to be treated in the main body of the present paper, the simultaneous presence of a solid and a liquid phase in thermodynamic equilibrium implies the chemical potentials in these phases to be equal for both components:

$$\mu_A^s = \mu_A^l, \tag{1}$$

$$\mu_B^s = \mu_B^l, \tag{2}$$

where μ is the chemical potential and l and s label the liquid phase and the solid phase, respectively. In terms of the activity a of the components A and B these equations become

$$\mu_A^{s*} + RT \ln a_A^s = \mu_A^{l*} + RT \ln a_A^l, \tag{3}$$

$$\mu_B^{s*} + RT \ln a_B^s = \mu_B^{l*} + RT \ln a_B^l, \tag{4}$$

where μ^* is the chemical potential of the pure compound. In these equations the implicit variables T, P and the compositions of the phases are omitted for convenience. Throughout the text it is assumed that the pressure is constant, say $P = P^{\Theta}$, that is, standard pressure and the temperature is considered as a variable.

2.1.1. S–L ideal phase diagrams

First the situation is considered for which the mixing is ideal both in the liquid and in the solid phase. This implies that in Eqs. (3) and (4) the activities can be replaced by the mole fractions

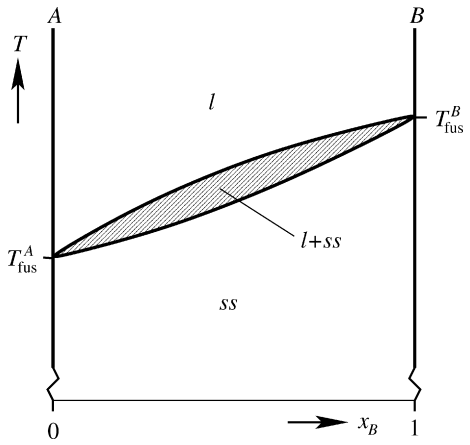

Fig. 1. Typical S–L phase diagram of a binary mixture, ideally mixing in both phases. The hatched area is forbidden because of Gibbs' phase rule; there the lever rule applies.

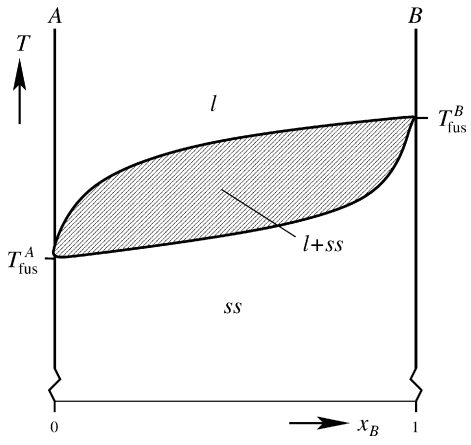

Fig. 2. Typical S–L phase diagram of a binary mixture for which the mixing is ideal, but the melting entropies of the pure compounds differ considerably. The hatched area is forbidden because of Gibbs' phase rule; there the lever rule applies.

($a_i^p = x_i^p; i = \text{A,B}; p = \text{s,l}$). Then, both in the liquid and in the solid phase the components A and B can be mixed in any ratio. For the solid phase this leads to a so-called solid solution. The resulting phase diagram is given in Fig. 1. The temperature T and the composition $x_\text{B} = 1 - x_\text{A}$ are the variables at the chosen pressure. At high temperatures one finds the well-mixed liquid phase, with no solid phase present. In this region the chemical potential of the solid phase is larger than that of the liquid phase for both compounds ($\mu_i^\text{s} > \mu_i^\text{l};\ i = \text{A,B}$). The stability domain for only a liquid phase is bounded from below by the liquidus line connecting the fusion temperatures of both (pure) components. Below the liquidus a solid solution starts being formed in combination with the liquid phase. In equilibrium, the compositions of these two phases follow the liquidus and the solidus (lower limiting line of the hatched area), respectively, on the right-hand and left-hand side of the hatched area. This implies that a composition in the hatched area is never realized.[1] The well-known lever rule determines the amounts of the liquid and solid phases. The size of the hatched area is determined by the fusion entropies and the difference in fusion temperatures of the two (pure) compounds. Below the solidus only the solid solution is present ($\mu_i^\text{s} < \mu_i^\text{l};\ i = \text{A,B}$). The ideal mixing phase diagram of Fig. 1 is typical for metals or semiconductors, for which the fusion entropies of the pure compounds are usually comparable. For organic crystals, even in case of ideal mixing behavior, the melting entropies can be quite different, leading to a more pronounced phase diagram. Fig. 2 shows an example of such a phase diagram, for which the two compounds still mix in all proportions in both phases.

2.1.2. S–L eutectic phase diagrams

Next the case that the compounds A and B are well miscible in the liquid phase but limited miscible in the solid phase, as a result of a relatively large positive enthalpy of mixing in the solid phase, is considered. This leads to solid solutions that are either rich in A, which are denoted as α or rich in B, denoted as β. In Fig. 3 the resulting eutectic phase diagram is drawn. For the eutectic composition, x_E, the liquid phase solidifies at T_E to form both solid solutions. For temperatures below the eutectic temperature, T_E, only two solid solution phases, α and β, are present each following the solidi. On the right-hand side of the solidus of compound B the system consists of a single solid solution (β) phase. The area on the left-hand side of the solidus of the compound A represents a single α phase. Note, that in the latter two areas, because of the presence of a single phase, Gibbs' phase rule allows both T and x_B as variables. In the hatched areas, again, the lever rule determines the amounts of the liquid and solid phases with compositions determined by the liquidus and solidi bordering these areas.

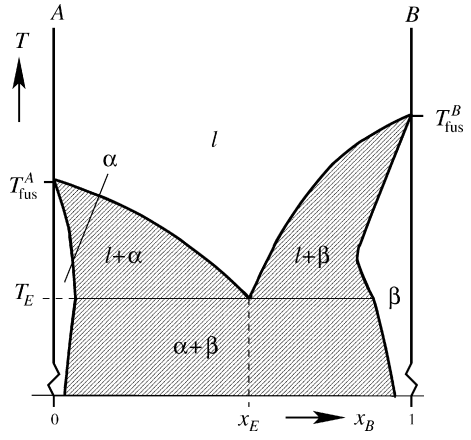

Fig. 3. S–L phase diagram of a binary mixture completely miscible in the liquid phase but almost immiscible in the solid phase. The hatched areas are forbidden because of Gibbs' phase rule; there the lever rule applies. Phase α is a solid solution rich in A and β is a solid solution rich in B.

[1] Gibbs' phase rule, $\mathcal{F} = \mathcal{C} - \mathcal{P} + 2$, for a two component system ($\mathcal{C} = 2$, namely A and B) and the presence of two phases ($\mathcal{P} = 2$, namely s and l) implies that for a chosen pressure P equilibrium is described by a curve in the (x_B, T)-diagram. As a consequence, in the hatched area two phases are present.

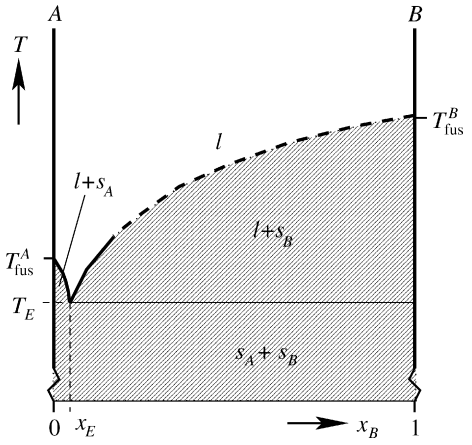

Fig. 4. Typical S–L phase diagram of a binary mixture well miscible in the liquid phase but immiscible in the solid phase. The hatched area is forbidden because of Gibbs' phase rule; there the lever rule applies. The dashed part of the liquidus of the solute B represents the solubility curve described in the present paper.

2.2. Solubility phase diagrams

Now, consider a solvent A in which a solute B is dissolved. A solubility curve is the curve $x(T)$ that describes the maximal amount of solute B that can be dissolved in the solvent A at a temperature T. In case of a typical solubility problem the fusion temperature of the solvent, T^A_{fus}, is relatively low as compared to that of the solute, that is, the solvent does not solidify within the temperature range relevant for the solution. Moreover, the solvent, in most cases, does not mix with the solute in its solid phase.[2] For such systems the phase diagram looks like that in Fig. 4. In this figure the solubility curve, which is nothing else than the liquidus line, is drawn as a dashed line. The solidus line of the solute is running along the $x_B = 1$-axis because of the assumption that the solid phase does not include solvent molecules. The solidus of the solvent is not drawn as it is not relevant because it is assumed that the temperature is always far above the fusion temperature of the solvent, T^A_{fus}. As a result, the solid phases are pure phases, either of compound A or B, denoted as s_A and s_B, respectively. Note, that the position of the eutectic composition, x_E, does not necessarily lie close to the $x_B = 0$-line. In terms of the phase diagram of Fig. 4, the present paper aims to describe the solubility curve for temperatures well above the eutectic temperature T_E, indicated as the dashed liquidus in the figure.

Thus, the solubility curve is nothing else than the line that in a $T(x)$ phase diagram divides the phase region consisting of a liquid mixture of A and B, for which no solid phase is present, and the region where a liquid mixture of A and B is present together with a pure solid phase of the solute B. In other words, thermodynamic equilibrium for a saturated solution is achieved when the solid phase B is in contact with a saturated solution at a given temperature T and pressure P. Equilibrium along the solubility curve implies that the chemical potential of the solute in the solid phase is equal to that of the solute in the liquid phase. In other words, thermodynamic equilibrium as described by Eqs. (3) and (4), for the case of a solubility curve is determined by

$$\mu_B^{s*} = \mu_B^{l*} + RT \ln a_B^l, \tag{5}$$

as the presence of a solid phase of the solvent A is not considered and the pure solid phase implies $a_B^s = 1$.

In terms of the activity coefficient γ_B^l and the mole fraction x_B^l of the solute in the solution Eq. (5) becomes

$$\mu_B^{s*} = \mu_B^{l*} + RT \ln \gamma_B x_B = \mu_B^{l*} + RT \ln x_B + RT \ln \gamma_B, \tag{6}$$

where the label l in the right-hand terms is omitted for convenience. This expression can be rearranged to find the solubility of the solute in terms of its mole fraction x_B:

$$\ln x_B = \frac{\mu_B^{s*} - \mu_B^{l*}}{RT} - \ln \gamma_B. \tag{7}$$

The second term on the right-hand side of Eq. (7) involves the generally very complex chemistry of the interactions between the solute and the solvent molecules. The first term on the right-hand side involves only properties of the pure solute, for which the difference in chemical potential can be described in terms of the Gibbs free energy difference (per mol) $g_B^* = G_B^*/n$, where n is the total number of moles in the system, according to

$$\frac{\mu_B^{s*} - \mu_B^{l*}}{RT} = \frac{g_B^{s*} - g_B^{l*}}{RT} = -\frac{\Delta_{s\to l} g_B^*(T)}{RT}. \tag{8}$$

The Gibbs free energy $\Delta_{s\to l} g_B^*(T)$ at the system temperature is not easily determined experimentally. Usually a thermodynamic cycle that is depicted in Fig. 5 is used for that (Hildebrand and Scott, 1964; Bennema and Söhnel, 1990; Gracin et al., 2002). In this figure, as an alternative for the direct path 1 → 4 which involves $\Delta_{s\to l} g_B^*(T)$, the solute is heated from the system temperature T to its fusion temperature (1 → 2), transformed to the liquid phase (2 → 3) and subsequently cooled down in the liquid state back to the system temperature (3 → 4), resulting in

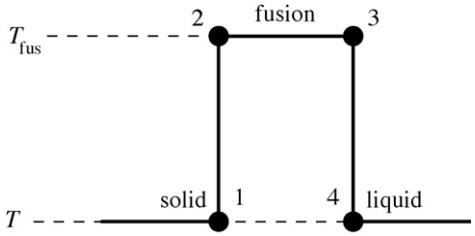

Fig. 5. Alternative thermodynamic cycle for the transition from the solid state of the solute to its undercooled liquid state at temperature T.

[2] Solvates are an exception to that; in the case of solvates the composition of the solid phase is fixed.

the supercooled liquid.[3] Conservation of free energy implies[4]

$$\Delta_{s\to l}g_B^*(T) = \Delta_{1\to 4}g_B^*(T) = \Delta_{1\to 2}g_B^* + \Delta_{2\to 3}g_B^* + \Delta_{3\to 4}g_B^*. \tag{9}$$

As at the melting temperature T_{fus} the liquid and solid phase are in thermodynamic equilibrium it follows that

$$\Delta_{2\to 3}g_B^* = \Delta_{fus}g_B^*(T_{fus}) = 0. \tag{10}$$

Combining Eqs. (8)–(10) results in

$$\frac{\mu_B^{s*} - \mu_B^{l*}}{RT} = -\int_T^{T_{fus}} d\left(\frac{g_B^{s*}}{RT'}\right) - \int_{T_{fus}}^{T} d\left(\frac{g_B^{l*}}{RT'}\right) = \frac{1}{R}\int_T^{T_{fus}} d\left(\frac{\Delta_{s\to l}g_B^*}{T'}\right). \tag{11}$$

In this equation T' is used as a dummy variable for the integration to avoid confusion with the system temperature T. Because the system is assumed to be at constant pressure P one can, subsequently, use (Gracin et al., 2002) the Gibbs–Helmholtz equation[5]

$$\left(\frac{\partial}{\partial T}\left(\frac{G}{T}\right)\right)_P = -\frac{H}{T^2}, \tag{12}$$

to rewrite expression (11) to

$$\frac{\mu_B^{s*} - \mu_B^{l*}}{RT} = -\frac{1}{R}\int_T^{T_{fus}} \left(\frac{\Delta_{s\to l}h_B^*}{T'^2}\right) dT'. \tag{13}$$

To obtain experimental values for this difference in chemical potential of the pure solute the transition enthalpy $\Delta_{s\to l}h_B^*$ has to be measured between the system temperature T and the melting temperature T_{fus}, which is still difficult but, in principle, more accessible than measuring the transition Gibbs free energies from Eq. (8) as $\Delta_{s\to l}h_B^*$ can be determined by measuring the heat of solidification of supercooled melts at various temperatures.

If Eq. (13) is combined with Eq. (7) one finds a general expression for the solubility of a solid phase B in a solvent A at temperature T and constant pressure P, under the assumption that the amount of A dissolved in the solid phase B is negligible, reading

$$\ln x_B = -\frac{1}{R}\int_T^{T_{fus}} \left(\frac{\Delta_{s\to l}h_B^*(T')}{T'^2}\right) dT' - \ln \gamma_B, \tag{14}$$

where $\Delta_{s\to l}h_B^*(T') = h_B^{l*}(T') - h_B^{s*}(T')$.

In Appendix A some approximations for the first term on the right-hand side of Eq. (14) are discussed. The second right-hand term in this expression, $\ln \gamma_B$, which describes the thermodynamics of the solute dissolved in the solvent as a deviation from ideal mixing, is generally rather involved. To include the effect of mixing the undercooled liquid phase of the solute B with the solvent A in the scheme of Fig. 5 the path has to be extended. The additional path 4 → 5 is drawn in Fig. 6. The path description used allows for an alternative formulation of Eq. (5)

$$\Delta_{1\to 4}\mu_B + \Delta_{4\to 5}\mu_B = \left(\mu_B^{l*} - \mu_B^{s*}\right) + \Delta_{mix}\mu_B = 0, \tag{15}$$

describing the equilibrium between the solid solute and the dissolved solute. Comparison with Eqs. (5) and (13) leads to

$$RT\ln a_B = RT\ln x_B + RT\ln \gamma_B = \Delta_{mix}\mu_B = -T\int_T^{T_{fus}} \left(\frac{\Delta_{s\to l}h_B^*}{T'^2}\right) dT'. \tag{16}$$

From a thermodynamic point of view there is an essential difference between mixtures of liquid phases or solid phases in equilibrium with their vapor mixtures and the solubility of a solid compound in a solvent. This becomes clear when one compares the mixing thermodynamics of an undercooled liquid phase of a solute in a solvent, which will be treated further on, with the mixture of two liquids. In the latter case one can establish thermodynamic equilibrium by mixing the two (or more) liquids by equating the chemical potentials of all components with their chemical potentials in the gas phase as is usually done for (L)iquid–(V)apor phase diagrams. For determining the solubility of a solid phase in a solvent, however, the mixing term depends, in general, not on the gas phase chemical potential (see footnote 1). In Fig. 6, one can *not* speak of an equilibrium between the undercooled solute and the solvent; only the final solution and the solid phase can be in thermodynamic equilibrium. This is expressed by Eq. (5) for the solute B. In that light the present models are a limited subset of the situations modeled by Pelton and Thompson (1975). In the latter paper the phase diagram of a binary system is studied in dependence of the mixing parameters both of the liquid and of the solid (solution) phase; in other words of solid–liquid equilibria.

In the following sections three models for the mixing term will be considered in more detail, namely ideal mixing, a regular solution model and a quasi-regular solution model. An important reference model is that of the ideal solution for which there is no enthalpy of mixing ($\Delta_{mix}^{ideal}H = 0$) and a mere mixing

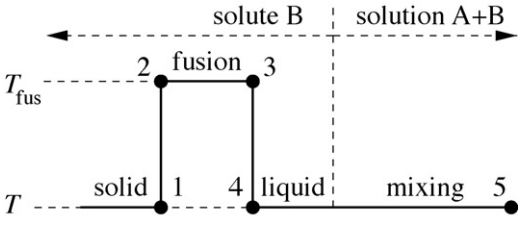

Fig. 6. Alternative thermodynamic cycle for the dissolution of a solid B in a solvent A at a temperature T.

[3] Prausnitz et al. (1999) consequently uses the triple point temperature T_{triple} instead of the fusion temperature T_{fus} because of the possible presence of a gas phase, implying a system pressure equal to the triple point pressure.

[4] If a solid state phase transition occurs before the meting point the Gibbs free energy change of that phase transition should be added in the cycle of Fig. 5; this is the case for a solute showing polymorphism which is treated in Section 3. In addition, if the solid sublimes before melting the sublimation transition should be used instead of the fusion transition.

[5] The Gibbs–Helmholtz equation, strictly spoken, only holds for equilibrium situations, that is, at T_{fus}; here, it is assumed that the equation also holds for $T < T' < T_{fus}$.

Table 1
The various approximations for the mixing enthalpy and entropy considered in the present paper; the athermal and general situation will not be discussed in detail

	$\Delta_{\rm mix}H$	$\Delta_{\rm mix}S$	$\Delta^{\rm E}_{\rm mix}H$	$\Delta^{\rm E}_{\rm mix}S$
Ideal	0	$\Delta^{\rm ideal}_{\rm mix}S$	0	0
Regular	$\Delta^{\rm reg}_{\rm mix}H$	$\Delta^{\rm ideal}_{\rm mix}S$	$\Delta^{\rm reg}_{\rm mix}H$	0
Athermal	0	$\Delta^{\rm ideal}_{\rm mix}S+\Delta^{\rm qu\text{-}reg}_{\rm mix}S$	0	$\Delta^{\rm qu\text{-}reg}_{\rm mix}S$
Quasi-regular	$\Delta^{\rm reg}_{\rm mix}H$	$\Delta^{\rm ideal}_{\rm mix}S+\Delta^{\rm qu\text{-}reg}_{\rm mix}S$	$\Delta^{\rm reg}_{\rm mix}H$	$\Delta^{\rm qu\text{-}reg}_{\rm mix}S$
General	$\Delta^{\rm E}_{\rm mix}H$	$\Delta^{\rm ideal}_{\rm mix}S+\Delta^{\rm E}_{\rm mix}S$	$\Delta^{\rm E}_{\rm mix}H$	$\Delta^{\rm E}_{\rm mix}S$

entropy contribution $\Delta^{\rm ideal}_{\rm mix}S$ representing the ideal configurational entropy of mixing. All deviations of this ideal solution model are covered by so-called excess contributions, defined as

$$\Delta^{\rm E}_{\rm mix}G=\Delta^{\rm E}_{\rm mix}H-T\Delta^{\rm E}_{\rm mix}S\equiv\Delta_{\rm mix}G-\Delta^{\rm ideal}_{\rm mix}G, \tag{17}$$

or

$$\Delta^{\rm E}_{\rm mix}H\equiv\Delta_{\rm mix}H\quad\text{and}\quad\Delta^{E}_{\rm mix}S\equiv\Delta_{\rm mix}S-\Delta^{\rm ideal}_{\rm mix}S. \tag{18}$$

In Table 1 an overview of the models is given.

2.3. Ideal solutions

Ideal solutions already offer a lot of insight in the problem of solubility. For an ideal solution, the solubility curve is the liquidus of the solute B of a phase diagram of two compounds A and B that are immiscible in the solid phase and perfectly miscible in the liquid phase. On a molecular level this implies that the reaction energy for the mixing reaction $\phi_{\rm AA}+\phi_{\rm BB}\rightarrow 2\phi_{\rm AB}$ between the solute and solvent molecules is zero

$$\phi_{\rm AB}-\frac{1}{2}(\phi_{\rm AA}+\phi_{\rm BB})=0, \tag{19}$$

where $\phi_{\rm AA}$ is the interaction energy between the solvent molecules, $\phi_{\rm BB}$ between the solute molecules and $\phi_{\rm AB}$ represents the heterogeneous interaction energy. In other words, $\Delta^{\rm ideal}_{\rm mix}H=0$. Then, the only contribution of the mixing to Eq. (16) is an ideal configurational entropic term, $\Delta^{\rm ideal}_{\rm mix}S$, as a result of the mixture of $n_{\rm A}$ mol of solvent and $n_{\rm B}$ mol of the (supercooled) liquid solute. The total Gibbs free energy of mixing is (Denbigh, 1981)

$$\Delta^{\rm ideal}_{\rm mix}G=-T\Delta^{\rm ideal}_{\rm mix}S=nRT(x_{\rm A}\ln x_{\rm A}+x_{\rm B}\ln x_{\rm B}), \tag{20}$$

where $n=n_{\rm A}+n_{\rm B}$. The ideal mixing contribution to the chemical potential change of the solute can be found by differentiating Eq. (20) with respect to $n_{\rm B}$ resulting in

$$\Delta^{\rm ideal}_{\rm mix}\mu_{\rm B}=\left(\frac{\partial\Delta^{\rm ideal}_{\rm mix}G}{\partial n_{\rm B}}\right)_{T,P,n_{\rm A}}=RT\ln x^{\rm ideal}_{\rm B}. \tag{21}$$

Substituting this result in Eq. (16) one obtains for the activity coefficient $\gamma_B=1$. Using Eq. (15) this leads to the ideal solubility equation

$$\ln x^{\rm ideal}_{\rm B}=\frac{\mu^{\rm s*}_{\rm B}-\mu^{\rm l*}_{\rm B}}{RT}=-\frac{1}{R}\int_T^{T_{\rm fus}}\left(\frac{\Delta_{\rm s\rightarrow l}h^*_{\rm B}(T')}{T'^{\,2}}\right)\mathrm{d}T'. \tag{22}$$

Note, that this solubility equation for an ideal solution only depends on pure solute parameters.

2.3.1. Interpretation of the ideal solubility curve

As long as it is assumed that the solution is ideal the solubility curve can be described by Eq. (22) for temperatures above the fusion temperature of the solvent and compositions with $x_{\rm B}>x_{\rm E}$. In most cases, for which $T^{\rm solv}_{\rm fus}\ll T^{\rm (B)}_{\rm fus}$, $x_{\rm E}$ is very small. As mentioned before, therefore, the solubility curve is considered to be represented by the liquidus of the solute for compositions in the range $0\lesssim x_{\rm B}<1$.

Assuming that the fusion enthalpy of the pure solute is independent of the temperature for all values of interest for $x_{\rm B}$, Eq. (22) reduces to

$$\ln x^{\rm ideal}_{\rm B}=-\frac{\Delta_{\rm fus}h^*_{\rm B}}{R}\left[\frac{1}{T}-\frac{1}{T_{\rm fus}}\right], \tag{23}$$

Eq. (23), when plotted as $\ln x$ versus $1/T$, a representation of solubility curves often referred to as van't Hoff curves, leads to a linear solubility curve which will be the reference curve in Section 2.4 dealing with regular solutions.

In the limit of very high concentrations, $x_{\rm B}\approx 1$, the solubility curve can be interpreted as a result of freezing point depression, the solvent acting as an impurity. Note that this approach is an alternative treatment of freezing point depression as it usually is considered for the case of a liquid with a dissolved solid or liquid acting as the impurity. For $x_{\rm B}\approx 1$ and using $\ln x_{\rm B}=\ln(1-x_{\rm A})\approx x_{\rm A}$ Eq. (23) becomes

$$T_{\rm fus}-T=\frac{RT^2_{\rm fus}}{\Delta_{\rm fus}h^*_{\rm B}}x_{\rm A}, \tag{24}$$

which is the standard equation for the linear freezing point depression, with the solvent acting as the impurity. As the solid is usually dissolved at temperatures T far below the fusion temperature $T_{\rm fus}$ the approximation used to arrive at Eq. (24) can usually not be made.

In practice, $\Delta_{\rm fus}h^*_{\rm B}$ will depend on temperature, as a result of which even for ideal solutions a classical solubility curve of $\ln x_{\rm B}$ versus $1/T$ does not result in a linear curve. In practice, however, the temperature range studied is rather limited, such that this curve is usually close to linear. In that case the slope of this curve should not be interpreted as $\Delta_{\rm fus}h^*_{\rm B}/R$ but rather as $\Delta_{\rm s\rightarrow l}h^*_{\rm B}(T_{\rm exp})/R$, sometimes denoted as $\Delta_{\rm diss}h_{\rm B}/R$, where $T_{\rm exp}$ represents the average experimental temperature (Boerrigter et al., 2002).

To get an impression of the more general case of an ideal solubility curve the temperature dependence of $\Delta_{\rm s\rightarrow l}h^*_{\rm B}(T)$ in Eq. (22) is considered in Appendix A in terms of a linear temperature dependence of the molar heat capacity according to

$$\Delta_{\rm s\rightarrow l}c_P(T)=c^{\rm l}_P(T)-c^{\rm s}_P(T)=\Delta c^0_P+\Delta c^1_P(T-T_{\rm fus}). \tag{25}$$

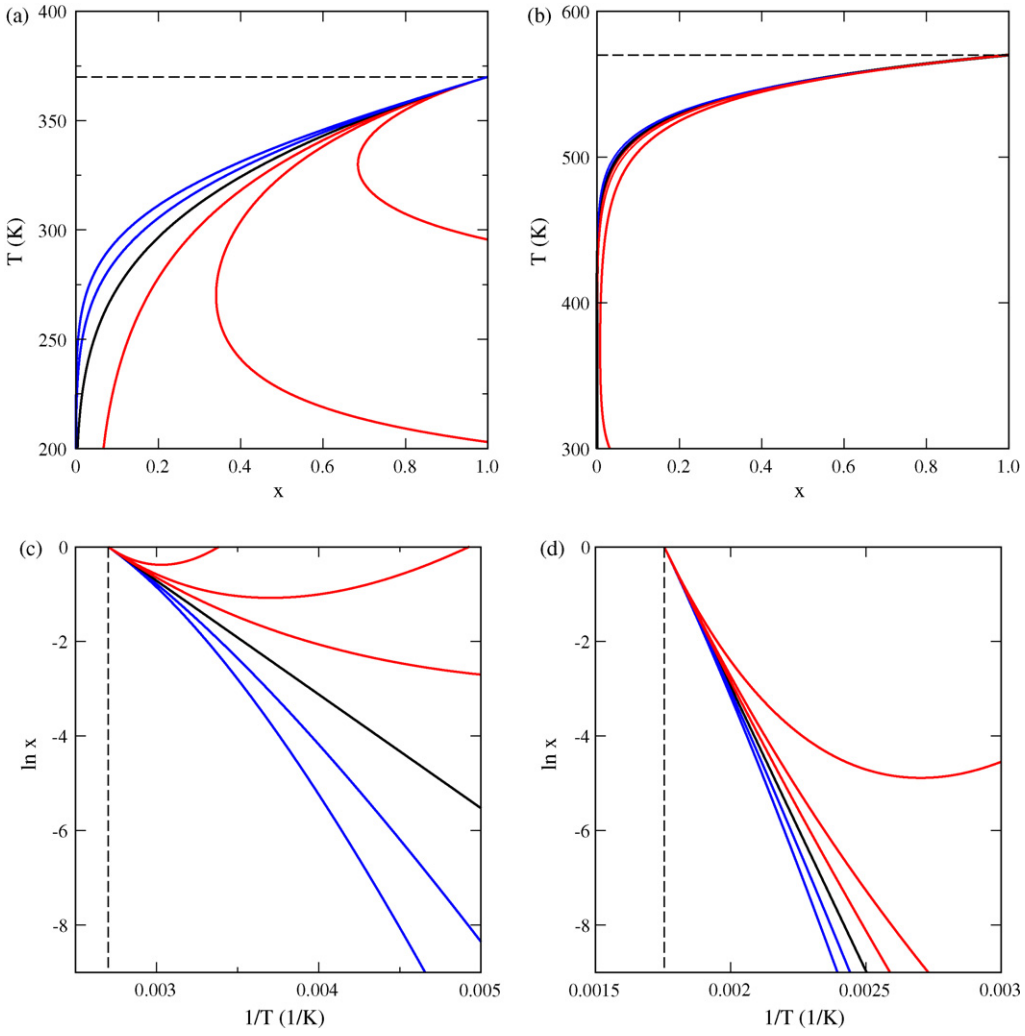

Fig. 7. The solubility curves according to Eq. (26) for (a) $\Delta_{\text{fus}}h^*_{\text{B}} = 20$ kJ/mol and $T_{\text{fus}} = 370$ K and (b) $\Delta_{\text{fus}}h^*_{\text{B}} = 100$ kJ/mol and $T_{\text{fus}} = 570$ K. The dashed black lines indicate T_{fus}. The heavy black lines represent the ideal solubility case for which Δc^0_P. The red lines show the values $\Delta c^0_P = 100$, 200 and 500 J/mol K and the blue lines $\Delta c^0_P = -100$ and -200 J/mol K, respectively. The figures (c) and (d) show the corresponding van't Hoff curves of (a) and (b), respectively.

Here the case for which $\Delta c^1_P = 0$ will be considered. Then Eq. (51) becomes

$$\ln x_{\text{B}} = \frac{\Delta_{\text{fus}}h^*_{\text{B}}}{R}\left[\frac{1}{T_{\text{fus}}} - \frac{1}{T}\right] + \frac{\Delta c^0_P}{R}\left[\frac{T_{\text{fus}}}{T} - \ln\frac{T_{\text{fus}}}{T} - 1\right]. \tag{26}$$

This equation is plotted for a few values for Δc^0_P in Fig. 7. The common point of the solubility curves in this figure is the fusion temperature of the pure solute, marked by the dashed black lines. For the limiting case that $T = T_{\text{fus}}$, Eq. (26) reduces to $\ln x_{\text{B}} = 0$, that is $x_{\text{B}} = 1$, corresponding to the pure liquid solute. The straight black lines in the van't Hoff plots (Fig. 7 c and d) represent the ideal solubility situation for $\Delta c_P = 0$. The red curves in Fig. 7 represent the situation for which $\Delta c^0_P > 0$. In that case the solubility is larger than the reference straight line, showing a minimum solubility for a temperature given by

$$T_{\text{min}} = T_{\text{fus}} - \frac{\Delta_{\text{fus}}h^*_{\text{B}}}{\Delta c^0_P} \quad (\Delta c^0_P > 0). \tag{27}$$

The blue curves show the situation for $\Delta c^0_P < 0$, resulting in a lower solubility and a non-linear van't Hoff curve as a result of the increasing contribution of the Δc^0_P term in Eq. (26) with decreasing temperature. A negative value for Δc^0_P is quite rare; an exception might have been found for pyrene (Wong and Westrum, 1971). Usually, $c^{\text{l}}_P(T) > c^{\text{s}}_P(T)$ for temperatures below the fusion temperature. Although a negative value for Δc^0_P is rare, a positive value for Δc^0_P large enough to lead to a minimum in the van't Hoff curve at an accessible temperature can not be ruled out, a priori. For temperatures $T < T_{\text{min}}$ the solubility increases with decreasing temperature. This phenomenon is known as retrograde solubility. The limiting case for which $x_{\text{B}} = 1$ below the fusion temperature, obviously, is non-physical. To get an idea of the quantitative effect of $\Delta_{\text{s}\to\text{l}}c_P(T)$ on the solubility curve the case of a pharmaceutical compound, venlafaxine, is considered in detail in Appendix B.

In conclusion, in almost all cases $\Delta_{\text{s}\to\text{l}}c_P(T) > 0$, leading to an increase in solubility and a deviation from the linear van't Hoff curve. For large positive values a minimum in the solubility can occur. Eq. (27) can be used as an indication for such behav-

ior. There are, however, other causes of retrograde solubility. In Section 2.6 the issue of retrograde solubility will be touched upon in more detail.

2.4. Regular solutions

As mentioned before, approximations for the solubility, or in general mixing of phases, beyond the ideal case are expressed in terms of excess contributions, like $\Delta^{\mathrm{E}}_{\mathrm{mix}}G$, $\Delta^{\mathrm{E}}_{\mathrm{mix}}H$ and $\Delta^{\mathrm{E}}_{\mathrm{mix}}S$, as in Eqs. (17) and (18). Accordingly, the excess mixing chemical potential difference is given by

$$\Delta^{E}_{\mathrm{mix}}\mu_{\mathrm{B}} = \left(\frac{\partial \Delta^{\mathrm{E}}_{\mathrm{mix}}G}{\partial n_{\mathrm{B}}}\right)_{T,P,n_{\mathrm{A}}} = \Delta_{\mathrm{mix}}\mu_{\mathrm{B}} - \Delta^{\mathrm{ideal}}_{\mathrm{mix}}\mu_{\mathrm{B}} = RT\ \ln\gamma_B. \tag{28}$$

Regular solutions[6] are a special case defined by the restriction that $\Delta^{\mathrm{E}}_{\mathrm{mix}}H \neq 0$ and $\Delta^{\mathrm{E}}_{\mathrm{mix}}S = 0$. On a molecular level this restriction implies that for the mixing reaction $\phi_{\mathrm{AA}} + \phi_{\mathrm{BB}} \rightarrow 2\phi_{\mathrm{AB}}$, it holds that $\phi_{\mathrm{AB}} \neq (1/2)(\phi_{\mathrm{AA}} + \phi_{\mathrm{BB}})$. For the limitations of regular solution models the reader is referred to Prausnitz et al. (1999).

The regular solution model treated here is based on the mean field model. In the mean field model it is assumed that the occurrence of the various interactions in the solution, ϕ_{AB}, ϕ_{AA} and ϕ_{BB} is randomly distributed, independent of the values of the interaction energies.[7] To simplify the statistics of the neighboring interactions further, the solvent is divided in cells which are either filled with a solute molecule B or a solvent molecule A. Each cell as Z interactions, with neighboring cells. Depending on the concentration of solute x_{B} the number of AB interactions, each having an energy ϕ_{AB}, between the cells in the model equals $Zx_{\mathrm{B}}x_{\mathrm{A}} = Zx_{\mathrm{B}}(1 - x_{\mathrm{B}})$. Therefore the total excess enthalpy now becomes

$$\Delta^{\mathrm{reg}}_{\mathrm{mix}}H = \Delta^{\mathrm{E}}_{\mathrm{mix}}H = Znx_{\mathrm{B}}\,(1 - x_{\mathrm{B}})\left[\phi_{\mathrm{AB}} - \frac{1}{2}\,(\phi_{\mathrm{AA}} + \phi_{\mathrm{BB}})\right], \tag{29}$$

where the superscript reg refers to the present mean field model for a regular solution and the molecular interaction energies are chosen to be negative. Defining the excess interaction energy by

$$\phi^{\mathrm{E}} \equiv \phi_{\mathrm{AB}} - \frac{1}{2}(\phi_{\mathrm{AA}} + \phi_{\mathrm{BB}}) \quad \text{and} \quad \Delta^{\mathrm{reg}}_{\mathrm{mix}}h \equiv Z\phi^{\mathrm{E}} \tag{30}$$

and combining Eqs. (20) and (29) one obtains

$$\Delta^{\mathrm{reg}}_{\mathrm{mix}}G = nx_{\mathrm{B}}\,(1 - x_{\mathrm{B}})\,\Delta^{\mathrm{reg}}_{\mathrm{mix}}h + nRT(x_{\mathrm{A}}\ \ln x_{\mathrm{A}} + x_{\mathrm{B}}\ \ln x_{\mathrm{B}}). \tag{31}$$

Differentiating this expression with respect to n_B one obtains for the chemical potential change of the solute

$$\Delta^{\mathrm{reg}}_{\mathrm{mix}}\mu_{\mathrm{B}} = \left(\frac{\partial \Delta^{\mathrm{reg}}_{\mathrm{mix}}G}{\partial n_{\mathrm{B}}}\right)_{T,P,n_{\mathrm{A}}} = \Delta^{\mathrm{reg}}_{\mathrm{mix}}h(1 - x_{\mathrm{B}})^2 + RT\ \ln x_{\mathrm{B}}. \tag{32}$$

Substituting this result in Eq. (16) one obtains for the solubility equation of the regular mean field solution

$$\ln x^{\mathrm{reg}}_{\mathrm{B}} = -\frac{1}{R}\int_{T}^{T_{\mathrm{fus}}}\left(\frac{\Delta_{\mathrm{s}\rightarrow\mathrm{l}}h^{*}_{\mathrm{B}}(T')}{T'^{\,2}}\right)\mathrm{d}T' - \frac{\Delta^{\mathrm{reg}}_{\mathrm{mix}}h}{RT}\left(1-x^{\mathrm{reg}}_{\mathrm{B}}\right)^2. \tag{33}$$

The activity coefficient in Eq. (16) is, thus, determined through

$$\ln\gamma_B = \frac{\Delta^{\mathrm{reg}}_{\mathrm{mix}}h}{RT}\left(1 - x^{\mathrm{reg}}_{\mathrm{B}}\right)^2. \tag{34}$$

To show the effect of $\Delta^{\mathrm{reg}}_{\mathrm{mix}}h$ on the solubility it will be assumed that $\Delta_{\mathrm{s}\rightarrow\mathrm{l}}h^{*}_{\mathrm{B}}$ is independent of temperature, implying

$$\ln x^{\mathrm{reg}}_{\mathrm{B}} = \frac{\Delta_{\mathrm{fus}}h^{*}_{\mathrm{B}}}{R}\left[\frac{1}{T_{\mathrm{fus}}} - \frac{1}{T}\right] - \frac{\Delta^{\mathrm{reg}}_{\mathrm{mix}}h_{\mathrm{B}}}{R}\left[\frac{\left(1 - x^{\mathrm{reg}}_{\mathrm{B}}\right)^2}{T}\right]. \tag{35}$$

This equation is plotted for a few values for $\Delta^{\mathrm{reg}}_{\mathrm{mix}}h_{\mathrm{B}}$ in Fig. 8. Again, the straight black lines in the van't Hoff plots (Fig. 8 c and d) represent the ideal solubility situation described by Eq. (23). The blue curves show the situation for $\Delta^{\mathrm{reg}}_{\mathrm{mix}}h_{\mathrm{B}} > 0$ which can, according to Eq. (29), be interpreted as $\phi_{\mathrm{AB}} > (1/2)(\phi_{\mathrm{AA}} + \phi_{\mathrm{BB}})$, a situation which is sometimes referred to as less than equivalent wetting, equivalent wetting referring to the ideal case. The red curves represent the situation for which $\phi_{\mathrm{AB}} < (1/2)(\phi_{\mathrm{AA}} + \phi_{\mathrm{BB}})$, or more than equivalent wetting. The reduced affinity between the molecules A and B for the blue curves leads to a lower solubility at a given temperature as compared to the ideal solubility curve. The reverse holds for the red curves.

In the limit of low concentrations of the solute, that is $x_B \rightarrow 0$, Eq. (35) becomes

$$\ln x^{\mathrm{reg}}_{\mathrm{B}} = \frac{\Delta_{\mathrm{fus}}h^{*}_{\mathrm{B}}}{R}\left[\frac{1}{T_{\mathrm{fus}}} - \frac{1}{T}\right] - \frac{\Delta^{\mathrm{reg}}_{\mathrm{mix}}h_{\mathrm{B}}}{RT}, \tag{36}$$

which in the van't Hoff plot leads to straight lines with a slope $(\Delta_{\mathrm{fus}}h^{*}_{\mathrm{B}} + \Delta^{\mathrm{reg}}_{\mathrm{mix}}h_{\mathrm{B}})/R$ instead of $\Delta_{\mathrm{fus}}h^{*}_{\mathrm{B}}/R$ for the ideal solubility curve, as can be seen in Fig. 8 c.

According to Eq. (35) the freezing point depression for small x_{A} becomes

$$T_{\mathrm{fus}} - T = \frac{RT^2_{\mathrm{fus}}}{\Delta_{\mathrm{fus}}h^{*}_{\mathrm{B}}}x_{\mathrm{A}} - \frac{\Delta^{\mathrm{reg}}_{\mathrm{mix}}h_{\mathrm{B}}T_{\mathrm{fus}}}{\Delta_{\mathrm{fus}}h^{*}_{\mathrm{B}}}x^2_{\mathrm{A}}, \tag{37}$$

showing an extra term as compared to Eq. (24).

Another important feature in Fig. 8 is that for large enough positive values of $\Delta^{\mathrm{reg}}_{\mathrm{mix}}h_{\mathrm{B}}$, the solubility curves show a horizontal plateau in the T versus x curves (Fig. 8 a and b). For these values of $\Delta^{\mathrm{reg}}_{\mathrm{mix}}h_{\mathrm{B}}$ a particular situation occurs. The solubility equation described by Eq. (23) would show a maximum

[6] The term regular solutions was first introduced by Hildebrand et al. (1970) and further restricted by Prausnitz et al. (1999).

[7] This assumption will obviously be too crude for situations where ϕ_{AB}, ϕ_{AA} and ϕ_{BB} differ too much.

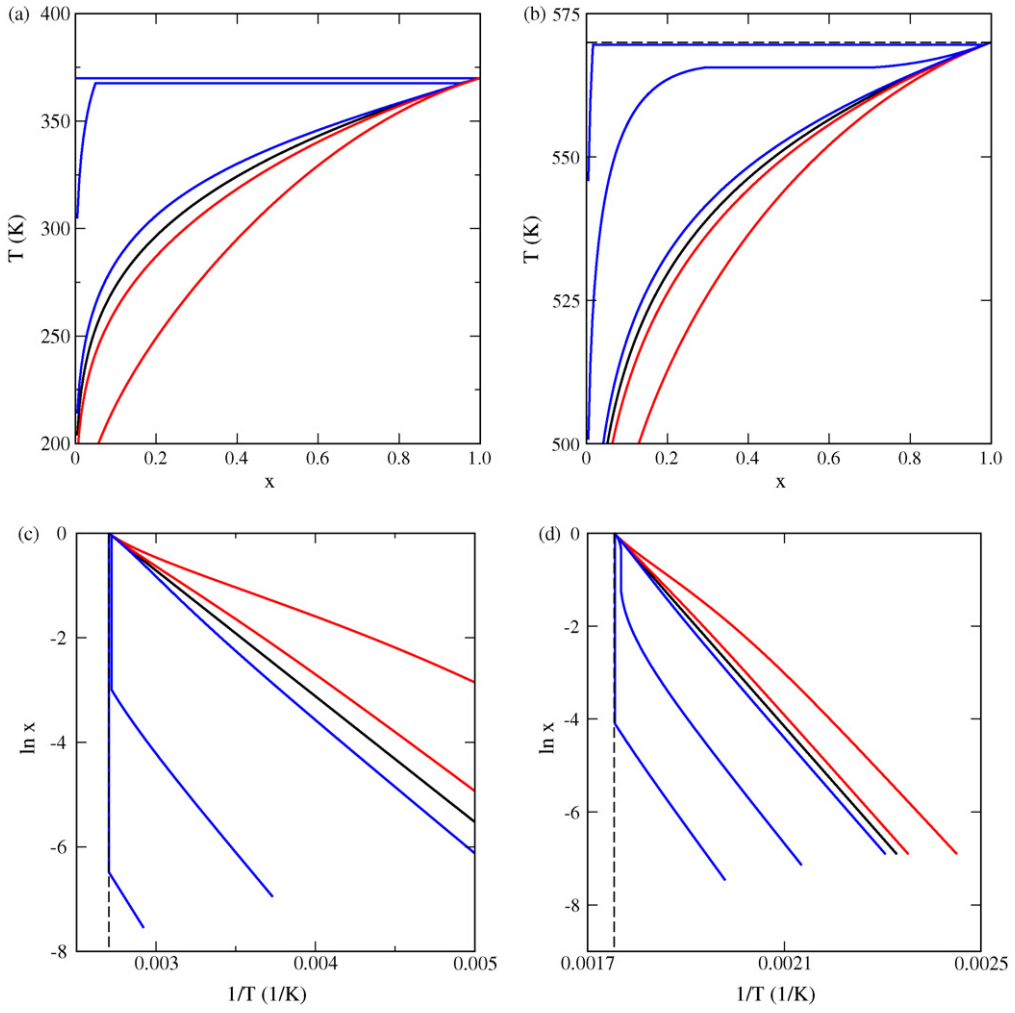

Fig. 8. The solubility curves according to Eq. (35) for (a) $\Delta_{\text{fus}}h_{\text{B}}^{*} = 20$ kJ/mol and $T_{\text{fus}} = 370$ K and (b) $\Delta_{\text{fus}}h_{\text{B}}^{*} = 100$ kJ/mol and $T_{\text{fus}} = 570$ K. The dashed black lines indicate T_{fus}. The heavy black lines represent the ideal solubility case for which $\Delta_{\text{mix}}^{\text{reg}}h_{\text{B}} = 0$. The blue lines show the values $\Delta_{\text{mix}}^{\text{reg}}h_{\text{B}} = 1$, 10 and 20 kJ/mol and the red lines $\Delta_{\text{mix}}^{\text{reg}}h_{\text{B}} = -1$ and -5 kJ/mol, respectively. The figures (c) and (d) show the corresponding van't Hoff curves of (a) and (b), respectively.

and a minimum in the x_{B} interval of the plateau. In between this maximum and minimum, however, the system is not stable due to liquid–liquid (L–L), separation, for which a diluted solution and a concentrated solution are in equilibrium. As a result, the solubility curve has to be replaced by the horizontal lines in an appropriate interval for the mole fraction x_{B}. According to Gibbs' phase rule for a two component system, considered here, three phases can only coexist for a single point in the (T, x) phase diagram. The end points of the horizontal lines correspond to two solutions in equilibrium with the solid phase of the solute. In the van't Hoff plots the L–L separation temperature corresponds to the vertical part in the blue lines. Often the term oiling out is used for L–L separation (Bonnett et al., 2003). The occurrence of L–L separation has not been reported often for molecular compounds. For pharmaceuticals this might be explained by the, often, classified information of the data, see e.g. (Deneau and Steele, 2005); a paper with full details on this topic was published by Lafferrère et al. (2004a, b). In case of protein crystallization, although strictly spoken not a binary system as a result of the presence of additional salts, L–L separation is a common feature often a result of kinetic effects (Vekilov, 2004). In Appendix C the thermodynamics behind the cause of L–L separation are explained; there, also the conditions for L–L separation for the present regular solution model will be given.

For negative values of $\Delta_{\text{mix}}^{\text{reg}}h_{\text{B}}$ no extrema are found in the solubility curve within the present model.

2.5. Beyond regular solutions

In the strict definition of a regular solutions as introduced by Hildebrand et al. (1970) the excess entropy of mixing, $\Delta_{\text{mix}}^{\text{E}}S$, is zero (cf. Table 1). In this section a non-zero term for $\Delta_{\text{mix}}^{\text{E}}S$ will be added to the regular solution model. For that it will be assumed that the excess entropy, like in the mean field model for the regular solution, will depend on the number of heterogeneous interactions between the solvent molecules A and the solute molecules B, leading to a Gibbs free energy of mixing equal to

$$\Delta_{\text{mix}}^{\text{qu-reg}}G = nRT\,(x_{\text{A}}\,\ln x_{\text{A}} + x_{\text{B}}\,\ln x_{\text{B}}) + nx_{\text{B}}\,(1 - x_{\text{B}})\left[\Delta_{\text{mix}}^{reg}h - T\Delta_{\text{mix}}^{\text{qu-reg}}s\right]. \quad (38)$$

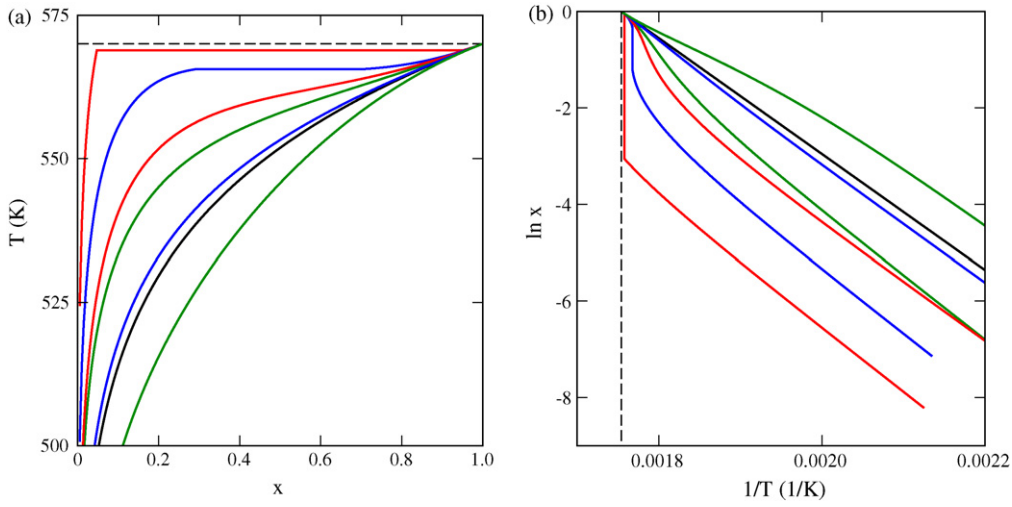

Fig. 9. The solubility curves according to Eq. (39) for $\Delta_{\mathrm{fus}}h_{\mathrm{B}}^{*} = 100$ kJ/mol and $T_{\mathrm{fus}} = 570$ K. The dashed black lines indicate T_{fus}. The heavy black lines represent the solubility case for which $\Delta_{\mathrm{mix}}^{\mathrm{reg}}h_{\mathrm{B}} = \Delta_{\mathrm{mix}}^{\mathrm{qu\text{-}reg}}s = 0$. The blue lines show the values $\Delta_{\mathrm{mix}}^{\mathrm{reg}}h_{\mathrm{B}} = 1$, 10 kJ/mol and $\Delta_{\mathrm{mix}}^{\mathrm{qu\text{-}reg}}s = 0$. The green curves show the corresponding situations for $\Delta_{\mathrm{mix}}^{\mathrm{qu\text{-}reg}}s = 10$ J/mol K; the red curves for $\Delta_{\mathrm{mix}}^{\mathrm{qu\text{-}reg}}s = -10$ J/mol K. (a) The (x, T)-diagram and (b) the corresponding van't Hoff curves.

This excess entropy term should therefore be interpreted as being mainly due to a change in the vibrational and rotational degrees of freedom of the molecules, but also containing extra configurational contributions. This model is sometimes referred to as the quasi-regular solution model, explaining the superscript in the equation (Stølen and Grande, 2004). Differentiating Eq. (38) with respect to n_{B} one finds analogously to the case of regular solutions, neglecting the temperature dependence of $\Delta_{\mathrm{s}\to\mathrm{l}}h_{\mathrm{B}}^{*}(T)$, for the solubility equation

$$\ln x_{\mathrm{B}}^{\mathrm{qu\text{-}reg}} = \frac{\Delta_{\mathrm{fus}}h_{\mathrm{B}}^{*}}{R}\left[\frac{1}{T_{\mathrm{fus}}} - \frac{1}{T}\right] - \left(\frac{\Delta_{\mathrm{mix}}^{\mathrm{reg}}h_{\mathrm{B}} - T\Delta_{\mathrm{mix}}^{\mathrm{qu\text{-}reg}}s}{R}\right)\left[\frac{\left(1 - x_{\mathrm{B}}^{\mathrm{reg}}\right)^{2}}{T}\right]. \quad (39)$$

The activity coefficient in Eq. (16), for the quasi-regular solution model, thus becomes $\ln\gamma_{\mathrm{B}} = \left(\Delta_{\mathrm{mix}}^{\mathrm{reg}}h/RT - \Delta_{\mathrm{mix}}^{\mathrm{qu\text{-}reg}}s/R\right)\left(1 - x_{\mathrm{B}}^{\mathrm{reg}}\right)^{2}$. The resulting solubility curves are plotted in Fig. 9 for a several of the parameters of Fig. 8 b and a realistic value of $\Delta_{\mathrm{mix}}^{\mathrm{qu\text{-}reg}}s = 10$ J/mol K. In the van't Hoff plots the slopes for the lower limit of x_{b} are still given by $(\Delta_{\mathrm{fus}}h_{\mathrm{B}}^{*} + \Delta_{\mathrm{mix}}^{\mathrm{reg}}h_{\mathrm{B}})/R$ as in the regular solution case. Comparing Figs. 8 b and d and 9 shows that positive values of the excess entropy suppress the deviation from ideality of the excess enthalpy, while negative values amplify the deviation.

A positive and negative value for the excess entropy can be interpreted as an increase, respectively decrease, in vibrational and rotational entropy in the solution as a result of the difference between the A–B interactions as compared to the A–A and B–B interactions. In other words, any excess enthalpy, either positive or negative, will imply a change in excess entropy. In many cases $\Delta_{\mathrm{mix}}^{\mathrm{reg}}h_{\mathrm{B}}$ and $\Delta_{\mathrm{mix}}^{\mathrm{qu\text{-}reg}}s$ have the same sign (Oonk et al., 1998) resulting in a mutually compensating effect in Eq. (39), which in turn leads to a smaller deviation from the ideal solubility curve.

2.6. Deviations from mean field models

In the previous two sections the solubility of solutes has been discussed on the basis of a mean field model assuming a random distribution of the solute and solvent molecules, with isotropic interaction between them. Relatively strong homogeneous interactions lead to clustering of A or B molecules resulting in deviations from the mean field approximation. The case of hydrogen bonds in solutions and complexes formed in electrolytic solutions are notorious for that. Both situations are not well described by the simple models presented here. More sophisticated models as referred to in the introduction deal with clustering effects, but are beyond the scope of this paper as they depend too much on the specific compound and solvent used. However, the special case of retrograde solubility will be treated briefly in the following section.

2.7. Retrogade solubility

As was pointed out in Section 2.3 retrograde solubility, i.e. decreasing solubility with increasing temperature within a certain temperature interval, can in exceptional cases be explained by a temperature dependence of the difference in heat capacity of the undercooled molten solute and the solid solute. Also the (quasi) regular solution models cannot describe this phenomenon without taking such a difference in heat capacity into account. In general two causes can be distinguished for retrograde solubility.

A difference in heat capacity, $\Delta_{\mathrm{s}\to\mathrm{l}}c_{P}(T)$, between the undercooled liquid phase and the solid phase of the solute as described in Section 2.3 might lead to a retrograde solubility. Although in Appendix B it is shown that this effect is not large enough for the case of the pharmaceutical compound venlafaxine, there might exist examples of more complex organic molecules for which $\Delta_{\mathrm{s}\to\mathrm{l}}c_{P}(T)$ is large enough. Eq. (27) shows that a retrograde solubility can be expected in case of a solute that has a relatively small heat of fusion $\Delta_{\mathrm{fus}}h^{*}$ combined with a large difference in

heat capacities $\Delta_{s\to l}c_P(T)$. Calculations similar to the ones performed in Appendix B, for fat crystals (SSS), e.g., showed a fully negligible effect of the relatively large value of $\Delta_{s\to l}c_P(T)$, ranging from 400 J/mol K at $T = 300$ K to 100 J/mol K at $T = T_{fus}$, caused by the large enthalpy of fusion, $\Delta_{fus}h^* = 196$ kJ/mol (Matovic et al., 2005). In general, a strong effect is to be expected for compounds that have a large number of degrees of freedom in the (undercooled) liquid phase as compared to the solid phase.

A decrease in entropy in the solution as a result of strong solvation interactions can also lead to retrograde solubility. Such an effect should be included in $\Delta^{E}_{mix}S$ with an appropriate temperature dependence. Examples are found for aqueous solutions of salts. Small cations like Li^+ and Ca^{2+} result in large ordered hydration shells leading to strong heterogeneous interactions between the solute and solvent. The same holds for some cases of transition metal ions forming complexes like Co^{4+} in the salt $[N(CH_3)]_2CoCl_4$. No retrograde solubilities were found to be reported for salts of pharmaceuticals, possibly because in most cases the counter ion is an anion for these salts.

Hexamethylenetetramine (HMT), used in explosives and plastics industries, is an example of a molecular crystal that shows retrograde solubility (Quadrifoglio et al., 1971; Blanco et al., 2006). The hydrate of the compound ($C_6H_{12}N_4{\cdot}6H_2O$) shows a eutectic behavior in the aqueous phase diagram, which dissolves incongruently at 286 K to form the anhydrate ($C_6H_{12}N_4$). The solubility curve of the anhydrate, although nearly temperature independent, is a retrograde (Aladko et al., in press). As a result of the presence of a haxahydrate, it is tempting to attribute the retrograde behavior to the formation of complexes with the solvent (Quadrifoglio et al., 1971); lack of thermodynamic data, makes it difficult to determine the effect of the heat capacity difference $\Delta_{s\to l}c_P(T)$.

There is another case of retrograde solubility, beyond the scope of this paper. In case of solid solutions the mixing thermodynamics of the solvent in the solute has to be included and one has to consider the Eqs. (3) and (4) instead of Eq. (5). Even for a regular solution model this leads to an additional term $\Delta^{reg}_{mix}H^s$, where the superscript s refers to the solid solution phase. This additional parameter is enough to lead to retrograde solubility as was shown for solid solutions of Sb and Cu in Si and Ge (Thurmond and Struthers, 1953). Such a retrograde solubility curve is visible in Fig. 3 for the solidus of the solid solution phase β. Solid solutions are quite common in alloys and mixtures of similar organic molecules like alkanes or fats (Oonk et al., 1998), but rarely observed for molecular crystals like pharmaceuticals dissolved in common solvents. If solid solutions play a role, retrograde solubilities can occur. Solid solutions should not be confused with solvates for which the solvent and solute are built-in in a stoichiometrical relation in the solid phase solvates, therefore lead to a very different phase diagram as will be discussed in Section 3.1.

3. Solubility and polymorphism

Polymorphism is the phenomenon that a compound, the solute B, can crystallize in more than one crystal structure under seemingly identical conditions. Although there is only one thermodynamically stable phase for a given temperature and pressure, often metastable crystalline phases are formed that can persist for long times. Eventually, these phases will transform to the stable phase. This behavior is usually interpreted in terms of Ostwald's rule of stages (Ostwald, 1897). If the solute exhibits polymorphism, the various polymorphic forms will have a different solubility. In general, the solubility of the metastable forms will be higher than that of the stable form. To keep the reasoning simple, situations of compounds showing only two polymorphic forms are discussed. The generalization to cases of more than two polymorphic forms is straightforward. The thermodynamics of polymorphic systems is treated in detail and illustrated with various experimental examples by Burger and Ramberger (1979a, b). Methods to determine the relative thermodynamic stability of polymorphs have been treated by Yu (1995) and Yu et al. (2005). The effect of kinetics that favors the formation of metastable forms is discussed in terms of metastable zones by Threlfall (1995). In terms of the thermodynamics of solutions there is an important difference between monotropic and enantiotropic polymorphism. For a monotropic system there is only one stable form at all temperatures at a given pressure. In that case, in thermodynamic equilibrium, the metastable phase will always be dissolved and the stable form can be in equilibrium with the solution as described by Eq. (5). For an enantiotropic polymorphic system, however, there is a phase transition temperature T_{trs} below which one of the two polymorphic forms (say form I) is stable and the other one is metastable, while above that temperature form II is stable and form I is metastable. This implies that at the temperature T_{trs} it holds that $\mu^s_{BI}(T_{trs}) = \mu^s_{BII}(T_{trs})$. Any polymorphic form has its own (metastable) S–L phase diagram. In case of an enantiotropic polymorphic compound B the equilibrium phase diagram shows an additional feature as depicted in Fig. 10 as compared to Fig. 4. At the transition temperature, T_{trs}, indicated as T^B_{trs} in Fig. 10 the solubility (liquidus) curves for the two polymorphs cross. In the latter figure the liquidi of both phase diagrams are only shown above the transition temperature. Only at the transition temper-

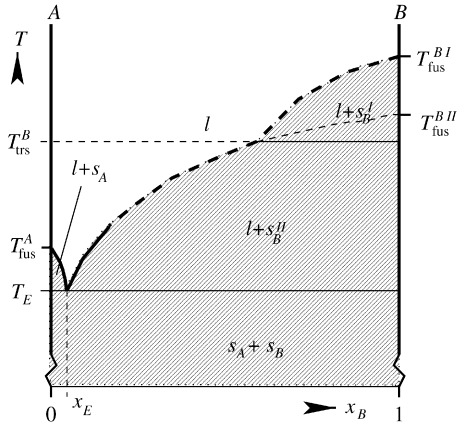

Fig. 10. Typical S–L phase diagram of a binary mixture well miscible in the liquid phase but immiscible in the solid phase, for an enantiotropic polymorphic system of the solute B. The dashed part of the liquidus of the solute B represents the solubility curve described in the present paper. At T^B_{trs} a solid–liquid phase transition between the polymorphic forms I and II occurs.

ature both polymorphic solid forms can be in equilibrium with the solution:

$$\mu^{s}_{BI}(T_{trs}) = \mu^{s}_{BII}(T_{trs}) = \mu^{l}_{B}(T_{trs}) = \mu^{l*}_{B}(T_{trs}) + RT\ \ln a^{l}_{B}(T_{trs}). \tag{40}$$

Note, that this equation is independent of the solvent used (Davey, 1982).[8] This implies that in thermodynamic equilibrium the solubility versus temperature curves of different polymorphs always cross each other at the same transition temperature T_{trs}. In this light, situations where concomitant polymorphism (Bernstein et al., 1999) is observed for temperatures that differ from the phase transition temperature T_{trs}, always represent non-equilibrium situations.

A further consequence of enantiotropic polymorphism is that for temperatures below the transition temperature the integral in Eq. (14) contains a contribution $\Delta_{trs}h^{*}_{B}(T_{trs})/T^{2}_{trs}$ for each of the models discussed above. For example, for the case that the difference in molar heat capacity is independent of the temperature between T and the fusion temperature of the solid phase melting at the highest temperature, Eq. (26) has to be replaced by

$$\ln x_B = \sum_{trs} \frac{\Delta_{trs}h^{*}_{B}}{RT_{trs}} + \frac{\Delta_{fus}h^{*}_{B}}{R}\left[\frac{1}{T_{fus}} - \frac{1}{T}\right] + \frac{\Delta_{s\to l}c_P}{R}\left[\frac{T_{fus}}{T} - \ln\frac{T_{fus}}{T} - 1\right] - \ln\gamma_B. \tag{41}$$

Although, strictly a non-equilibrium situation, the presence of the metastable polymorphic form in a solution, possibly concomitant with the stable polymorph, can, in many cases, persist for a long time; long enough to determine a solubility curve (x versus T) for both polymorphic forms. Such cases are found both for monotropic (Aret et al., 2007; Stoica et al., 2005) and enantiotropic (Park et al., 2003) systems. In principle, a metastable polymorph corresponds to a local minimum in the Gibbs free energy. The metastable solid phase cannot find kinetic pathways to transform to the stable form in the time allowed by the experiment. The solubility of both polymorphs can, therefore, be described by Eq. (7), be it with the appropriate parameters for the two polymorphs according to

$$\ln x_{BI(II)} = \frac{\mu^{s*}_{BI(II)} - \mu^{l*}_{B}}{RT} - \ln\gamma_B. \tag{42}$$

Note, that the term $\ln\gamma_B$, describing the non-ideality of the solution, is the same for both polymorphs at any temperature T; the same holds for the chemical potential of the pure liquid solute, μ^{l*}_{B}. This implies that the difference in solubility of the two polymorphs at a temperature T offers valuable information of the difference in chemical potential of their solid phases

$$\mu^{s*}_{BII} - \mu^{s*}_{BI} = RT\left[\ln x_{BII} - \ln x_{BI}\right]. \tag{43}$$

As this equation involves pure compounds the chemical potentials can be rewritten in terms of the differences in enthalpy and entropy of the two polymorphs according to

$$\Delta_{II\to I}h^{*} - T\Delta_{II\to I}s^{*} = RT\Delta_{II\to I}\ln x_B. \tag{44}$$

Assuming a negligible temperature dependence for both $\Delta_{II\to I}h^{*}$ and $\Delta_{II\to I}s^{*}$,[9] this equation can be used to determine $\Delta_{II\to I}h^{*}$ and $\Delta_{II\to I}s^{*}$ as the slope and intercept with the y-axis in a $\Delta\ln x_B$ versus $1/RT$ plot for the temperatures considered. This was used, for example by Stoica et al. to determine the dissolution enthalpy and entropy of two polymorphic forms of a steroid (Stoica et al., 2005). Moreover, Eq. (44) implies that the transition temperature for an enantiotropic system is determined by

$$T_{trs} = \frac{\Delta_{II\to I}h^{*}}{\Delta_{II\to I}s^{*}} \tag{45}$$

as for any equilibrium phase transition. This temperature, when neglecting the difference in heat capacity between the two polymorphs in the temperature range between the transition temperature T_{trs} and T_{fus}, is given by

$$T_{trs} = \frac{\Delta_{fus}h^{*}_{BII} - \Delta_{fus}h^{*}_{BI}}{(\Delta_{fus}h^{*}_{BII}/T^{II}_{fus}) - (\Delta_{fus}h^{*}_{BI}/T^{I}_{fus})} \tag{46}$$

Therefore the transition temperature can, besides from solubility curves, be estimated from DSC measurements as long as no solid–liquid transition between the polymorphic forms occurs during such an experiment. This has been successfully applied to three enantiotropically related polymorphs of venlafaxine (van Eupen et al., in press).

In case the transition can not be avoided and the transition temperature T_{trs} and the corresponding enthalpy change $\Delta_{trs}h^{*}$ are available, e.g. from accurate DSC experiments, one can use this information to estimate the solubility ratio of the polymorphs using the method described by Mao et al. (2005).

3.1. Pseudo polymorphs and solvates

The term pseudo polymorphism was originally used for crystal structures that can contain guest molecules in various amounts, e.g. solvent molecules, not influencing the structure of the host lattice. Solvates are crystals for which the crystal structure contains a stoichiometric amount of solvent molecules at well-defined crystallographic positions. In the case of water being the solvent the term hydrates is used. Solvates can therefore be considered as compounds of the form A_pB_q, where A represents the solvent and B the pure solute. In the field of polymorphism the term pseudo polymorphs is often used referring to solvates. Fig. 11 shows a typical composition-temperature phase diagram of such a system for which, two solid phases are stable: a pure solid phase B and a solvate AB. As before, the solid phase

[8] Here it is assumed that surface free energy contributions as a result of solvent–solid interactions can be neglected, which is, usually, reasonable for practical crystal sizes, even in the case of precipitation. For most molecular crystals the surface energy becomes comparable to the bulk energy for crystal diameters of the order of some 1–10 nm.

[9] Note, that this assumption is much more realistic as compared to the assumptions discussed when considering freezing point depression as it only concerns temperatures for which the solubility curves are determined, which are usually far below the fusion temperature of the solute.

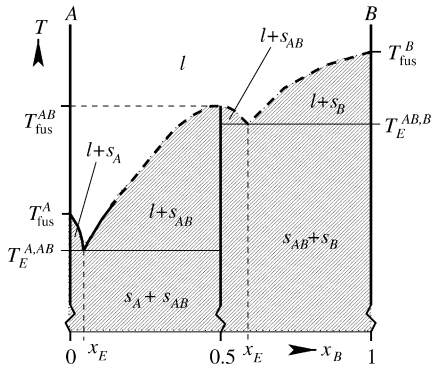

Fig. 11. Typical S–L phase diagram of a binary mixture well miscible in the liquid phase but only stoichiometrically miscible in the solid phases, leading to a pure solid phase B and a solvate *AB*; in case of molecular crystals such a solvate is often called a pseudo polymorph.

of the solvent A is not considered as it is out of the experimental temperature range as indicated by the dashed solubility curves. The maxima in the solubility curves correspond to the fusion temperatures of the solid phases. Starting from these maxima the solubility curves can, again, be considered as freezing point depression curves as a result of the admixture of one of the other phases to the liquid phase, the curves ending in the eutectic points x_E at the temperatures $T_E^{A,\,AB}$ and $T_E^{AB,\,B}$, respectively. Within the hatched areas the lever rule can be applied to determine the amounts of the two phases in equilibrium. In Fig. 11 the phase diagram limited to the composition interval $0 < x_B < 0.5$ can be interpreted as an S–L phase diagram comparable to that of Fig. 4 with B replaced by *AB*; a same comparison can be made for the interval $0.5 < x_B < 1$, A and B being replaced by *AB* and B, respectively. Concentrating on the composition interval $0.5 < x_B < 1$ the negative slope of the solubility curve bounding the $l + s_{AB}$ region should not be interpreted as a retrograde solubility in this case. In practice, more than one solvate or pseudo polymorphic form can be stable in various temperature and composition intervals, leading to as so many maxima and eutectic points in the phase diagram (Reutzel-Edens et al., 2003).

4. Conclusion

Although many methods have been developed for a quantitative prediction of vapor liquid equilibrium (VLE) phase diagrams in the last century, much less attention has been given to solid liquid equilibria (SLE). SLE phase diagrams contain the essential information for determining the solubility of a compound in a solvent. Solubility has been studied in great detail at the beginning of the last century. The thermodynamic basis of solubility theory seems to have lost attention since then. In the last few decades solubility of especially organic molecules has regained interest as a result of the discovery of many new organic molecules in the field of pharmaceuticals. Not only the synthesis and purification of these compounds ask for suitable solvents and therefore solubility data, but also the frequent appearance of various polymorphic crystal forms of these compounds, often related to the solubility properties in different solvents, have led to an increasing demand for reliable solubility data.

In this paper the thermodynamic basis of solubility theory is reviewed and the link with binary phase diagrams is emphasized for that. Starting from the simplest solubility model, i.e. the ideal solubility case, models with increasing complexity are treated. For that a mean field approach is used. The resulting solubility curves as a function of temperature are presented for various values of the relevant thermodynamic parameters. Special situations, like liquid–liquid separation (oiling out) and retrograde solubility are highlighted. It is, for example, shown that the difference in heat capacity between an undercooled melt and the solid, a parameter which is almost always neglected, in the case of more complex molecules like many pharmaceuticals, can have a considerable effect on the solubility. Special attention is given to the solubility phase diagrams of monotropic and enantiotropic polymorphic forms as well as solvates (pseudo polymorphs). In passing a new method is introduced that allows to estimate the transition temperature of enantiotropically related polymorphs from melting temperatures and enthalpies of the polymorphs, which can be determined using standard calorimetric techniques.

Acknowledgment

We would like to acknowledge Dr. Rob Geertman for fruitful discussions and suggestions.

Appendix A. The pure solute parameters

The general solubility Eq. (14) involves a pure solute parameter, $\Delta_{s\to l}\mu_B^*$, according to

$$\frac{\Delta_{s\to l}\mu_B^*(T)}{RT} = \frac{\mu_B^{l*}(T) - \mu_B^{s*}(T)}{RT} = \frac{1}{R}\int_T^{T_{fus}} \left(\frac{\Delta_{s\to l}h_B^*(T')}{T'^2}\right) dT'. \quad (47)$$

Although, as mentioned before, $\Delta_{s\to l}h_B^*$ can be determined as a function of the temperature by measuring the heat of solidification of the supercooled liquid, various approximations have been made in the literature to come to an expression in terms of an experimentally more accessible parameter. Usually, such approximations are made for the molar heat capacity c_P, rather than for $\Delta_{s\to l}h_B^*$. Therefore, first Eq. (14) is rewritten (Gracin et al., 2002) in terms of the molar heat capacity c_P, using $h(T') = h(T_{fus}) + \int_{T_{fus}}^{T'} c_P\,dT$ as

$$\ln x_B = \frac{\Delta_{fus}h_B^*}{R}\left[\frac{1}{T_{fus}} - \frac{1}{T}\right] - \frac{1}{R}\int_T^{T_{fus}} \left(\frac{\int_{T_{fus}}^{T'} \Delta_{s\to l}c_P dT''}{T'^2}\right) dT', \quad (48)$$

where $\Delta_{s\to l}c_P = c_P^l - c_P^s$; Eq. (48) applies as long as the solute does not sublime before melting and there is no solid state phase transition between T and T_{fus}. The term $\ln\gamma_B$ is set equal to zero as only the pure solute terms are considered in this appendix. In Eq. (48) the first term on the right-hand side describes the

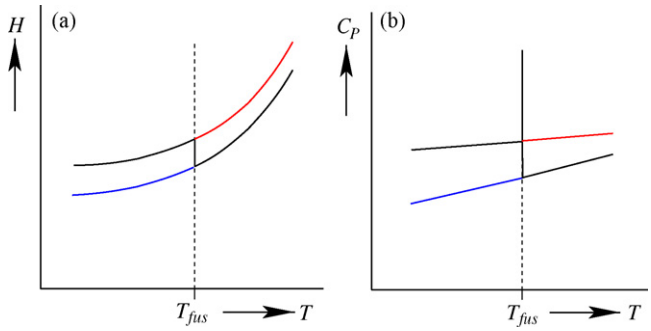

Fig. A.1. Schematic illustration of the fusion transition of the solid B; the red and blue curves represent the properties of the stable liquid and solid phase, respectively; the black curves represent the equilibrium properties of the solute. (a) The enthalpy of the solute. (b) The heat capacity of the solute in case of a quadratic temperature dependence of the enthalpy; the sharp peak at $T = T_{\text{fus}}$ is an idealized representation of the phase transformation.

contribution to the solubility due to the jump in the enthalpy as a result of the fusion process at the fusion temperature; the second term accounts for the differences in enthalpy going from the temperature T to T_{fus}. In Fig. A.1 these contributions are illustrated. The sharp peak in Fig. A.1 b and the corresponding jump in Fig. A.1 a mark the phase transformation and are an idealization of the more spread behavior found in calorimetric measurements. In practice, the transition from the solid to the liquid phase always starts immediately at T_{fus} during heating, while the liquid phase can, often, be undercooled below the fusion temperature. Therefore, the difference in heat capacity $\Delta_{\text{s}\to\text{l}}c_P$ cannot be determined above the fusion temperature, while for temperatures below T_{fus} a non-zero value can be measured. The temperature dependence of $\Delta_{\text{s}\to\text{l}}c_P$ from T to T_{fus} is described by the second term on the right-hand side of Eq. (48). Although the temperature dependence of the heat capacity of the solid phase and the undercooled liquid phase can be far from linear it is to be expected that the difference of these, that is $\Delta_{\text{s}\to\text{l}}c_P$, is only moderately dependent on the temperature. Below, some of the approximations found in the literature for the temperature dependence of $\Delta_{\text{s}\to\text{l}}c_P$ are mentioned.

Eq. (23) describes the solubility curve when the difference in molar heat capacity is neglected between T and T_{fus}, leading to a linear relation between $\ln x_{\text{B}}$ and $1/T$ in a classical solubility plot for ideal solutions.

Often an expansion of the difference in molar heat capacity for both phases, in powers of the temperature T, around T_{fus} is made. Here, only a linear dependence on the temperature as suggested in Fig. A.1 b, according to

$$\Delta_{\text{s}\to\text{l}}c_P(T) = c_P^{\text{l}}(T) - c_P^{\text{s}}(T) = \Delta c_P^0 + \Delta c_P^1\,(T - T_{\text{fus}}) \tag{49}$$

is considered. This leads to a quadratic temperature dependence of the difference in molar enthalpy according to

$$\Delta_{\text{s}\to\text{l}}h_{\text{B}}^*(T) = \Delta_{\text{fus}}h_{\text{B}}^* + \Delta c_P^0\,(T - T_{\text{fus}}) + \frac{\Delta c_P^1}{2}(T - T_{\text{fus}})^2. \tag{50}$$

Substituting Eq. (50) in Eq. (47) leads to the ideal solubility equation

$$\ln x_{\text{B}} = \frac{\Delta_{\text{fus}}h_{\text{B}}^*}{R}\left[\frac{1}{T_{\text{fus}}} - \frac{1}{T}\right] + \frac{\Delta c_P^0}{R}\left[\frac{T_{\text{fus}}}{T} - \ln\frac{T_{\text{fus}}}{T} - 1\right] + \frac{\Delta c_P^1 T_{\text{fus}}}{2R}\left[\frac{T}{T_{\text{fus}}} - \frac{T_{\text{fus}}}{T} + 2\ln\frac{T_{\text{fus}}}{T}\right]. \tag{51}$$

The non-zero difference in enthalpy at the transition temperature T_{fus} is covered by the first term on the right-hand side of the equation. In all these approximations the temperature is limited to $T \le T_{\text{fus}}$ and it is assumed that the transition to the liquid phase is instantaneous, or in other words, the temperature is increased slowly enough to allow the solid to melt in the experimental time. For a discussion of the effects of too fast temperature runs in a DSC experiment the reader is referred to Defossemont et al. (2004).

Appendix B. C_P-contribution: venlafaxine as an example

To get an impression of the contribution of the difference in molar heat capacity of the undercooled liquid and the crystal, $\Delta_{\text{s}\to\text{l}}c_P(T)$, to the solubility expression (26) the heat capacities for venlafaxine (van Eupen et al., in press) were measured using a Mettler Toledo DSC822$^{\text{e}}$. For that measurement 15 mg of venlafaxine was loaded to one of the calorimeter cups, the reference vessel left empty. The material was > 99.9 % grade. The sample was heated at a rate of 10° min^{-1} starting from room temperature up to a temperature well above the melting temperature ($T_{\text{fus}} = 348.1$ K), subsequently cooled down to a temperature at which the undercooled melt did not recrystallize yet. Starting from that temperature a second heating run was performed, again, up to a temperature well above the melting temperature. To determine the heat capacities accurately, the measurement

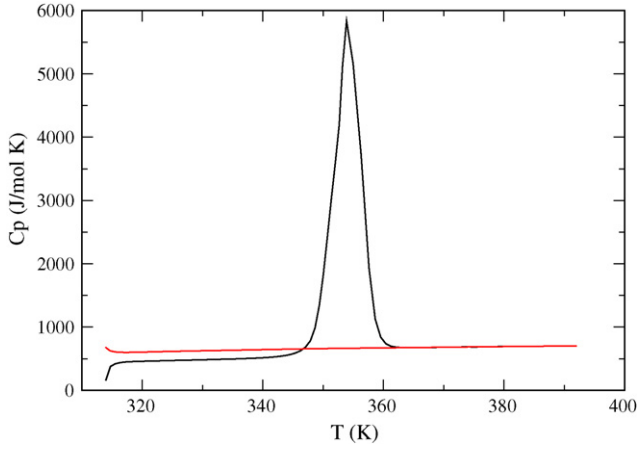

Fig. B.1. The measured C_P-curves of venlafaxine for a heating run (black trace) starting at room temperature up to a temperature well beyond the melting temperature ($T_{\text{fus}} = 348.1$ K), followed by a cooling run down to a temperature at which recrystallization did not occur (not shown). The second heating run (red trace) for the undercooled melt was made again up to temperatures well beyond the melting temperature; the deviations at low temperatures are an artifact of the measurement.

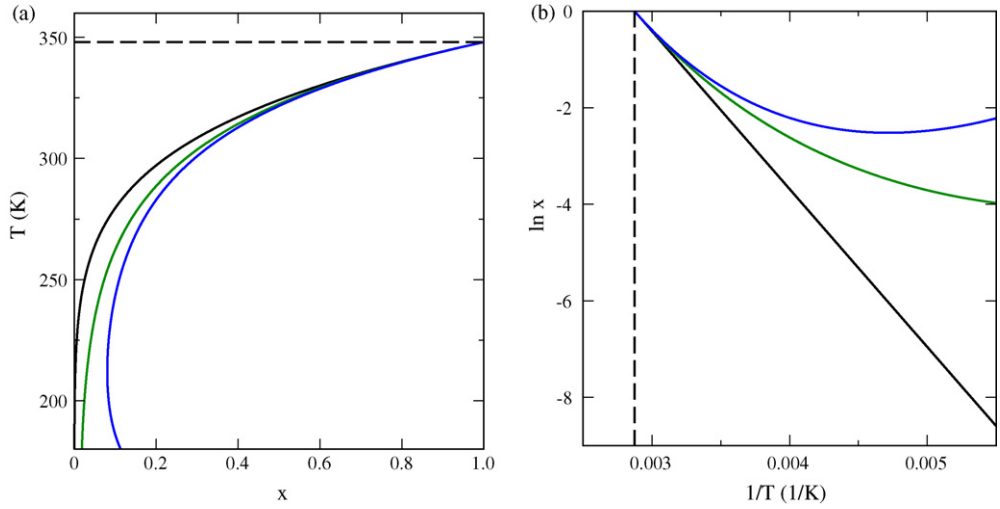

Fig. B.2. The solubility curves according to Eq. (26) for venlafaxine using $\Delta_{\text{fus}}h^*_{\text{B}} = 27.20$ kJ/mol and $T_{\text{fus}} = 348.1$ K. The heavy black curve represents the ideal solubility case for which $\Delta c^0_P = 0$. The green line shows the results for venlafaxine for which Δc^0_P was determined to be 145 J/mol K. For comparison the blue curve shows the case for $\Delta c^0_P = 200$ J/mol K. The dashed black line indicates T_{fus}. Figure (b) shows the corresponding van't Hoff curves of (a).

was preceded by two runs using the same cups; one performed for two empty cups and a second one for which one of the vessels was loaded with Al_2O_3 as a reference sample. The final temperature dependence of the C_P-value of venlafaxine was determined using the equation

$$C_{P,\text{sample}}(T) = \frac{\text{HF}_{\text{sample}} - \text{HF}_{\text{empty}}}{\text{HF}_{\text{Al}_2\text{O}_3} - \text{HF}_{\text{empty}}} \frac{m_{\text{Al}_2\text{O}_3}}{m_{\text{sample}}} C_{P,\text{Al}_2\text{O}_3}(T), \quad (52)$$

where HF is the measured heat flow as a function of the temperature and m is the mass of the sample. The resulting curves are shown in Fig. B.1. The deviations at low temperatures are an artifact due to the non-reliable data obtained with the device used at the start of any heating run. Undercooled venlafaxine can be cooled down to a temperature of approximately 310 K without solidification. The difference in heat capacity between solid venlafaxine and its undercooled liquid phase turns out to be almost independent of temperature over the entire range from 310 K up to T_{fus} and is determined to be $\Delta_{\text{s}\to\text{l}}c_P(T) \approx \Delta c^0_P = 145$ J/mol K. Using this value together with $T_{\text{fus}} = 348.1$ K and $\Delta_{\text{fus}}h^*_{\text{B}} = 27.20$ kJ/mol in Eq. (26), the effect of $\Delta_{\text{s}\to\text{l}}c_P(T)$ on the solubility can be calculated. In Fig. B.2 the results are shown. The figure shows that for the case of venlafaxine the solubility deviates considerably from the ideal solubility curve for which $\Delta c^0_P = 0$. Moreover, it shows that for somewhat larger values for Δc^0_P retrograde solubility can occur within an accessible temperature range.

As a second example, for naphthalene the same measurement was performed, although its liquid phase could be undercooled only some 10 degrees below its fusion temperature. In this case $\Delta_{\text{s}\to\text{l}}c_P(T)$ is relatively small and slightly increases with decreasing temperature. The estimated average value of $\Delta_{\text{s}\to\text{l}}c_P(T) \approx 20$ J/mol K leads only to a very small deviation from the ideal solubility curve as can be seen in Fig. B.3

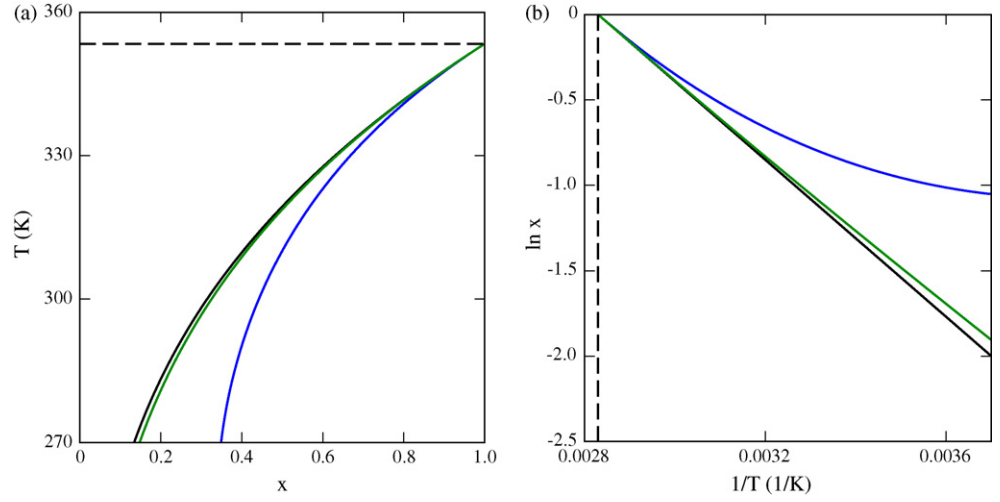

Fig. B.3. The solubility curves according to Eq. (26) for naphthalene using $\Delta_{\text{fus}}h^*_{\text{B}} = 19.1$ kJ/mol and $T_{\text{fus}} = 353.4$ K. The heavy black curve represents the ideal solubility case for which $\Delta c^0_P = 0$, the green line the case of naphthalene for which $\Delta c^0_P \approx 20$ J/mol K. For comparison the blue curve shows the case for $\Delta c^0_P = 200$ J/mol K. The dashed black line indicates T_{fus}. Figure (b) shows the corresponding van't Hoff curves of (a).

Appendix C. Liquid–liquid separation

In the regular solution model discussed in Section 2.4, Fig. 8 a and b show a horizontal plateau in the solubility curves beyond a critical positive value of $\Delta_{\mathrm{mix}}^{\mathrm{reg}} h_{\mathrm{B}}$. For the corresponding temperature the solubility curves have to be replaced by horizontal lines in the (x, T) diagrams, resulting in the coexistence of an A-rich and a B-rich solution in thermodynamical equilibrium with the solid phase. The coexistence of two liquid phases is also known as liquid–liquid (L–L) separation. Here, the thermodynamics behind L–L separation will be reviewed shortly. In Fig. C.1 a and b the solubility curve according to Eq. (35) for two of the curves in Fig. 8 b have been redrawn without the horizontal lines. According to Eqs. (32) and (35) the solubility curve describes the dependence of the chemical potential of the solute in the liquid phase, $\Delta_{\mathrm{mix}}^{\mathrm{reg}} \mu_{\mathrm{B}}$, on the mole fraction x_{B} up to a constant. As a result of the minimum free energy in thermodynamic equilibrium, it holds that

$$\left(\frac{\partial^2 G}{\partial n_{\mathrm{B}}^2}\right)_{P,T,n_{\mathrm{A}}} = \left(\frac{\partial \mu_{\mathrm{B}}^{\mathrm{l}}}{\partial n_{\mathrm{B}}}\right)_{P,T,n_{\mathrm{A}}} \geq 0 \tag{53}$$

as has been demonstrated in detail by Landau and Lifshitz (1959). The equality in Eq. (53) corresponds to a set of critical points, that define the borders of an instable situation. Substituting Eq. (32) one obtains for this equality condition

$$T = \frac{2\Delta_{\mathrm{mix}}^{\mathrm{reg}} h}{R} x_{\mathrm{B}} (1 - x_{\mathrm{B}}). \tag{54}$$

The corresponding curves, known as spinodals, have been drawn as the green lines in the (x, T) diagrams of Fig. C.1 a and b. Note, that these spinodals describe the behavior of the liquid phase. In case of the presence of also a solid phase B, the critical points intersect with the solubility curve at certain temperatures, exactly in the extrema of the solubility curve. In between these minimum and maximum values the slope of the solubility curves is negative, which therefore corresponds to a thermodynamically instable situation. The red curves in Fig. C.1 a and b correspond to the values in the (x, T) diagram where $\Delta_{\mathrm{mix}}^{\mathrm{reg}} \mu_{\mathrm{B}} = 0$ or, in other words, the Gibbs free energy of mixing in the liquid phase is minimal. These curves are defined by

$$T = \frac{\Delta_{\mathrm{mix}}^{\mathrm{reg}} h}{R} \frac{2x_{\mathrm{B}} - 1}{\ln(1 - x_{\mathrm{B}}) - \ln x_{\mathrm{B}}} \tag{55}$$

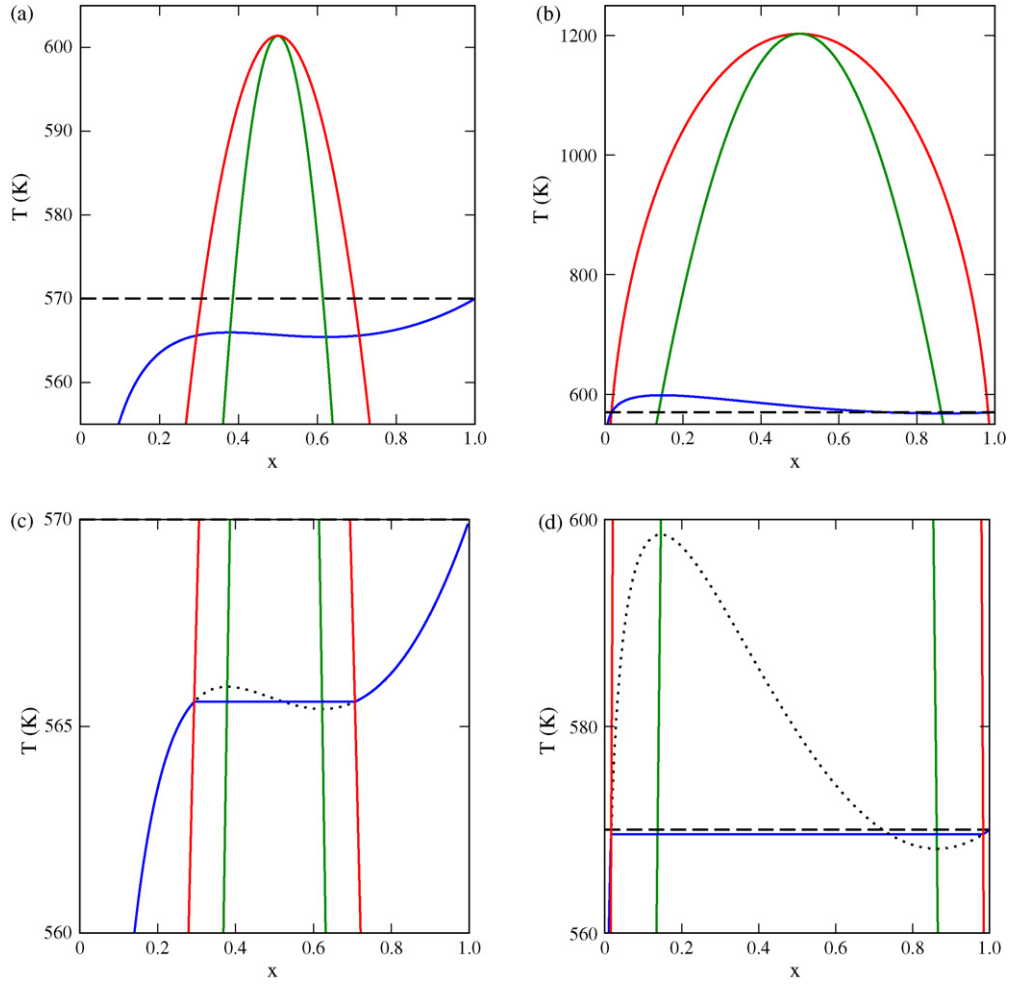

Fig. C.1. Two of the solubility curves (blue lines) of Fig. 8 b according to Eq. (35); $\Delta_{\mathrm{fus}} h_{\mathrm{B}}^{*} = 100\,\mathrm{kJ/mol}$ and $T_{\mathrm{fus}} = 570\,\mathrm{K}$. The red lines show the function of Eq. (55), the green lines that of Eq. (54) for (a) $\Delta_{\mathrm{mix}}^{\mathrm{reg}} h_{\mathrm{B}} = 10\,\mathrm{kJ/mol}$ and (b) $\Delta_{\mathrm{mix}}^{\mathrm{reg}} h_{\mathrm{B}} = 20\,\mathrm{kJ/mol}$. Note, the different ranges for T in (a) and (b). The graphs (c) and (d) show an enlarged vertical scale for (a) and (b), respectively; in these graphs the metastable solubility lines are indicated as dotted black lines.

and known as the binodals. For a liquid mixture without a solid phase present, the binodal defines the region in the (x, T) diagram below which L–L separation takes place. When also a solid phase is present, in the present case the solid B, Gibbs' phase rule restricts this region to a single temperature, which is defined by the intersection between the binodal and the solubility curve. The values of x_B of the two intersection points cannot be determined in an analytical form because it involves a transcendental equation. These have been determined numerically for the parameters of Fig. C.1 a and b, leading to the Fig. C.1 c and d where the vertical scale has been blown up to show the intersection points more clearly and the horizontal lines in the corrected blue solubility curve have been added.[10]

The binodal and spinodal in the present model are symmetrical in x_A and x_B. The top of both at $x_B = 1/2$ is given by

$$T = \frac{\Delta^{\text{reg}}_{\text{mix}} h}{2R}. \tag{56}$$

Substituting this value in the solubility Eq. (35) one finds for the critical value of $\Delta^{\text{reg}}_{\text{mix}} h$ for L–L separation

$$\Delta^{\text{reg}}_{\text{mix}} h = \frac{4\Delta_{\text{fus}} h^*_B}{2\ln 2 - 1 + 2(\Delta_{\text{fus}} h^*_B / RT_{\text{fus}})}, \tag{57}$$

which for the parameters of Fig. C.1 yields $\Delta^{\text{reg}}_{\text{mix}} h = 9.392$ kJ/mol, which is slightly smaller than the middle blue curve in the figure.

In Section 2.5 an additional excess entropy was introduced leading to a so-called quasi-regular solution model in the mean-field approximation. For this model the binodal and spinodal are still symmetrical in x_A and x_B. The top of both at $x_B = 1/2$ is now given by

$$T = \frac{\Delta^{\text{reg}}_{\text{mix}} h}{\Delta^{\text{qu-reg}}_{\text{mix}} s + 2R}, \tag{58}$$

leading to a critical value of $\Delta^{\text{reg}}_{\text{mix}} h$ for L–L separation

$$\Delta^{\text{reg}}_{\text{mix}} h = \frac{4\Delta_{\text{fus}} h^*_B (1 + 2\Delta^{\text{qu-reg}}_{\text{mix}} s/R)}{2\ln 2 - 1 + 2(\Delta_{\text{fus}} h^*_B / RT_{\text{fus}})}, \tag{59}$$

For the parameters of Fig. 9 this leads to $\Delta^{\text{reg}}_{\text{mix}} h = 15.040$ kJ/mol for $\Delta^{\text{qu-reg}}_{\text{mix}} s = 10$ J/mol K. This explains the absence of a plateau, indicating L–L separation, in Fig. 9 a for $\Delta^{\text{reg}}_{\text{mix}} h = 10$ kJ/mol and $\Delta^{\text{qu-reg}}_{\text{mix}} s = 10$ J/mol K.

Summarizing, only at the temperature where the solubility curve intersects the binodal two liquid phases with mole fractions corresponding to the intersection points are in thermodynamic equilibrium with the solid phase of the solute B. For temperatures and mole fractions above the solubility curve but below the binodal (red line) the liquid also separates in two liquid phases, with no solid phase. For temperatures and mole fractions above the binodal only a single liquid phase is present.

[10] Note, that within the L–L separation interval for x_B the areas of the deviating solubility above and below the horizontal line are not equal, in contrast to the well-known example of the liquid–gas phase equilibrium of, e.g. the van der Waals equation, where the so-called 'Maxwell equal area rule' holds.

References

Aladko, L.S., Komarov, V.Y., Manakov, A.Y., Ancharov, A.I., in press. J. Incl. Phenom. Macrocycl. Chem.

Aret, E., Meekes, H., Vlieg, E., Deroover, G., 2007. Dyes Pigments 72, 339.

Arlt, W., Spuhl, O., Klamt, A., 2004. Chem. Eng. Process. 43, 221.

Barton, A.F.M., 1975. Chem. Rev. 75, 731.

Bennema, P., Söhnel, O., 1990. J. Cryst. Growth 102, 547.

Bernstein, J., Davey, R.J., Henck, J.-O., 1999. Angew. Chem. Int. Ed. 38, 3440.

Blanco, L.H., Sanabria, N.R., Dávila, M.T., 2006. Therm. Chim. Acta 450, 73.

Boerrigter, S.X.M., van den Hoogenhof, C.J.M., Meekes, H., Bennema, P., Vlieg, E., van Hoof, P.J.C.M., 2002. J. Phys. Chem. B 106, 4725.

Bonnett, P.E., Carpenter, K.J., Dawson, S., Davey, R.J., 2003. Chem. Commun., 698–699.

Burger, A., Ramberger, R., 1979a. Mikrochim. Acta II, 273.

Burger, A., Ramberger, R., 1979b. Mikrochim. Acta II, 259.

Davey, R.J., 1982. Solvent effects in crystallisation processes. In: Current Topics in Material Sciences. North-Holland.

Defossemont, G., Randzio, S.L., Legendre, B., 2004. Cryst. Growth Design 4, 1169.

Denbigh, K., 1981. The Principles of Chemical Equilibrium. Cambridge University Press.

Deneau, E., Steele, G., 2005. Or. Proc. Res. & Dev. 9, 943.

Eckert, F., Klamt, A., 2002. AIChE J. 48, 369.

Fiege, C., Joh, R., Petri, M., Gmehling, J., 1996. J. Chem. Eng. Data 41, 1431.

Gmehling, J.G., Anderson, T.F., Prausnitz, J.M., 1978. Ind. Eng. Chem. Fundam. 17, 269.

Gmehling, J., 2003a. Pure Appl. Chem. 75, 875.

Gmehling, J., 2003b. Fluid Phase Equilibr. 210, 161.

Gracin, S., Brinck, T., Rasmuson, Å., 2002. Ind. Eng. Chem. Res. 41, 5114.

Hansen, C.M., 1969. Ind. Eng. Chem. Prod. Res. Dev. 8, 2.

Hildebrand, J.H., Scott, R.L., 1964. The Solubility of Nonelectrolytes. Dover, New York.

Hildebrand, J.H., Prausnitz, J.M., Scott, R.L., 1970. Regular and Related Solutions. Van Nostrand Reinhold Company.

Hildebrand, J.H., 1916. J. Am. Chem. Soc. 38, 1452.

Hildebrand, J.H., 1929. J. Am. Chem. Soc. 51, 66.

Jacques, J., Collet, A., Wilen, S.H., 1994. Enantiomers, Racemates and Resolutions. Krieger, FL.

Jakob, A., Joh, R., Rose, C., Gmehling, J., 1995. Fluid Phase Equilbr. 113, 117.

Lafferrère, L., Hoff, C., Veesler, S., 2004a. J. Crystal Growth 269, 550.

Lafferrère, L., Hoff, C., Veesler, S., 2004b. Cryst. Growth Design 4, 1175.

Landau, L.D., Lifshitz, E.M., 1959. Course of Theoretical Physics, vol. 5: Statistical Physics. Pergamon Press.

Lohmann, J., Röpke, T., Gmehling, J., 1998. J. Chem. Eng. Data 43, 856.

Lohmann, J., Joh, R., Gmehling, J., 2001. Ind. Eng. Chem. Res. 40, 957.

Los, J.H., Matovic, M., 2005. J. Phys. Chem. B 109, 14632.

Los, J.H., van Enckevort, J.P., Vlieg, Elias, Flöter, E., Gandolfo, F., 2002. J. Phys. Chem. B 106, 7331.

Los, J.H., van Enckevort, W.J.P., Meekes, H., Vlieg, E., 2007. J. Phys. Chem. B 111, 782.

Mao, C., Pinal, R., Morris, K.R., 2005. Pharm. Res. 22, 1149.

Matovic, M., van Miltenburg, J.C., Los, J.H., Gandolfo, F.G., Flöter, E., 2005. J. Chem. Eng. Data 50, 1624.

Mortimer, F.S., 1922. J. Am. Chem. Soc. 44, 1416.

Oonk, H.A.J., Mondieig, D., Haget, Y., Cueveas-Diarte, M.A., 1998. J. Chem. Phys. 108, 715.

Ostwald, W., 1897. Z. Phys. Chem. 12, 289.

Park, K., Evans, J.M.B., Meyerson, A.S., 2003. Cryst. Growth Design 3, 991.

Pelton, A.D., Thompson, W.T., 1975. Prog. Solid State Chem. 10, 119.

Prausnitz, J.M., Lichtenthaler, R.N., de Avezedo, E.G., 1999. Molecular Thermodynamics of Fluid-Phase Equilibria, 3rd ed. Prentice-Hall PTR, Upper Saddle River, NJ.

Quadrifoglio, F., Crescenzi, V., Cesàro, A., Delben, F., 1971. J. Phys. Chem. 75, 3633.
Reutzel-Edens, S.M., Bush, J.K., Magee, P.A., 2003. Cryst Growth Design 3, 897.
Ruelle, P., Fariña-Cuendet, A., Kesselring, U.W., 2000. Perspect. Drug Discov. 18, 61.
Stølen, S., Grande, T., 2004. Chemical Thermodynamics of Materials. John Wiley & Sons Ltd., Chichester, England.
Stoica, C., Tinnemans, P., Meekes, H., Vlieg, E., van Hoof, P.J.C.M., Kaspersen, F.M., 2005. Cryst. Growth Design 5, 975.
Threlfall, T.L., 1995. Analyst 120, 2435.
Thurmond, C.D., Struthers, J.D., 1953. J. Phys. Chem. 57, 831.
van Eupen, J.Th.H. et al., in preparation.
van Eupen, J.Th.H., Elffrink, W.W.J., Keltjens, R., Bennema, P., de Gelder, R., Smits, J.M.M., van Eck, E.R.H., Kentgens, A.P.M., Deij, M.A., Meekes, H., Vlieg, E., Cryst. Growth Design, in press.
Vekilov, P.G., 2004. Cryst. Growth Design 4, 671.
Wong, W.K., Westrum, E.F., 1971. J. Chem. Therm. 3, 105.
Yu, L., 1995. J. Pharm. Sci. 84, 966.
Yu, L., Huang, J., Jones, J., 2005. J. Phys. Chem. 109, 19915.